Pharmacological Characterization of TAS05567, a Potent and Selective Inhibitor of Spleen Tyrosine Kinase, in Animal Models of Inflammatory Diseases and B-cell Malignancies

January 2019

Hiroaki Hayashi

Pharmacological Characterization of TAS05567, a Potent and Selective Inhibitor of Spleen Tyrosine Kinase, in Animal Models of Inflammatory Diseases and B-cell Malignancies

A Dissertation Submitted to
the School of the Integrative and Global Majors,
the University of Tsukuba
in Partial Fulfillment of the Requirements
for the Degree of Doctor of Philosophy in Disease Mechanism
(Doctoral Program in Life Science Innovation)

Hiroaki HAYASHI

List of Contents

List of Abbreviation

ABC:	activated B-cell subtypes
ACR:	American College of Rheumatology
BCR:	B-cell receptor
BLNK:	B-cell linker protein
BSA:	bovine serum albumin
Btk:	Bruton's tyrosine kinase
CAIA:	collagen antibody-induced arthritis
CAPS:	cryopyrin-associated periodic syndromes
CIA:	collagen-induced arthritis
COMP:	cartilage oligomeric matrix protein
DMARDs:	disease-modifying anti-rheumatic drugs
DLBCL:	diffuse large B-cell lymphoma
DNP:	2,4-dinitrophenyl
ELISA:	enzyme-linked immunosorbent assay
ERK:	extracellular Signal-regulated Kinase
FBS:	fetal bovine serum
FcR:	Fc receptor
FL:	follicular lymphoma
GCB:	germinal center B-cell
IC50:	inhibitory concentration 50
ICs:	immune complexes
IL:	interleukin
Igs:	immunoglobulins
ITP:	immune thrombocytopenic purpura
IVIg:	intravenous immunoglobulin
JAK:	Janus kinase
LPS:	lipopolysaccharide
M-CSF:	macrophage colony-stimulating factor
MMP:	matrix metalloproteinase
NHL:	non-Hodgkin lymphoma
PE:	phycoerythrin
PLC:	phospholipase C
RA:	rheumatoid arthritis
RANK:	receptor activator of nuclear factor kappa-B

RANKL:	RANK ligand
RPMI:	Roswell Park Memorial Institute
RT:	room temperature
SD:	standard deviation
SEM:	standard error of the mean
siRNA:	small interfering RNA
Syk:	spleen tyrosine kinase
TNF:	tumor necrosis factor
TNP:	2,4,6-trinitrophenol
TRAP:	tartrate-resistant acid phosphate
VEGFR:	vascular endothelial growth factor receptor
WM:	Waldenström's macroglobulinemia

Abstract

Spleen tyrosine kinase (Syk) is a non-receptor cytoplasmic tyrosine kinase that is primarily expressed by cells of hematopoietic lineage. Syk acts downstream of immunoreceptor tyrosine-based activation motif–coupled receptors, including the B-cell receptor (BCR) and FcRs, and influences diverse biological events, such as cytokine production, degranulation, differentiation, and proliferation, suggesting that Syk is profoundly involved in the development of autoimmune diseases, allergic diseases, and malignancies. For example, direct injection of Syk small interfering RNA (siRNA) into the limb joints prevents joint swelling in models of autoantibody-induced arthritis. Regarding the relationship with allergic reactions, Syk-deficient mast cells fail to degranulate and secrete mediators when stimulated through FcεRI. Furthermore, Syk silencing by siRNA leads to a dramatic decrease of cell viability of B-cell chronic lymphocytic leukemia. Considering its biological actions and association with the pathogenesis of inflammatory diseases and B-cell malignancies, pharmacologic inhibition of Syk represents a potential therapeutic intervention option for patients with these diseases. Indeed, several ATP-competitive Syk inhibitors, notably fostamatinib, have already been evaluated in clinical trials performed in patients with autoimmune

diseases, including rheumatoid arthritis (RA) and immune thrombocytopenic purpura (ITP). Even though fostamatinib was efficacious against chronic refractory ITP, it is unclear whether inhibition of Syk activity specifically contributed to the clinical response and adverse events observed in the clinical trials, as this drug inhibits several kinases, including vascular endothelial growth factor receptor (VEGFR) 2 and Janus kinase (JAK) 2. Another Syk inhibitor, entospletinib, has been developed for the treatment of leukemia, but it inhibits multiple protein kinases within 100-fold of its inhibitory concentration 50 (IC50) value for Syk. These findings suggest that novel Syk inhibitors with different activity profiles from the above-mentioned inhibitors are required to provide new therapeutic options. Against this background, we tried to identify a novel, potent, and selective orally available Syk inhibitor. Investigation of structure-activity relationships led to identification of TAS05567 from chemically synthesized Syk inhibitory compounds. We characterized the profile of TAS05567 using biochemical assays as well as cell-based assays and showed its therapeutic potential for autoimmune diseases in Chapter 1. We further assessed the therapeutic potential of our compound for other diseases, including type 1 allergic diseases as well as B-cell malignancies, using preclinical animal models in Chapter 2. TAS05567 potently inhibited the activity of Syk, showing an average IC50 of 0.37 nM in enzymatic assays.

TAS05567 was more potent than R406 (an active metabolite of fostamatinib), exhibiting an average IC50 of 13 nM. The specificity of TAS05567 for Syk was determined at 50 nM (approximately 140 times the IC50 value) using a panel of 192 kinases. In these analyses, TAS05567 only showed >70% inhibition of Syk and 4 other kinases, while R406 at 500 nM (approximately 40 times its IC50 for Syk) showed >70% inhibition of 43 kinases. In addition, the IC50 values of TAS05567 and R406 were determined for VEGFR2 and JAK2. Whereas TAS05567 showed at least 10-fold selectivity for Syk over the 4 kinases, R406 showed equal or greater efficacy against these kinases. Next, we evaluated the effectiveness of TAS05567 in blocking the BCR-dependent signaling cascade using B-cell line. TAS05567 was marked inhibition of the phosphorylation of BLNK (IC50 = 1.8 nM), PLCγ2 (IC50 = 23 nM), and Erk1/2 (IC50 = 9.8 nM) induced by anti-IgM. TAS05567 also showed stronger inhibition of these molecules in the BCR-dependent signaling cascade than R406. In addition, we evaluated the inhibitory effects of TAS05567 on FcγR-mediated TNF-α release by macrophages. TAS05567 showed concentration-dependent inhibition of TNF-α production by IgG stimulation. Syk also contributes directly to bone resorption in RA via its kinase activity–mediated regulation of receptor activator of nuclear factor kappa-B (RANK) signaling pathway that is essential for differentiation of osteoclasts. TAS05567 strongly inhibited the

formation of mature osteoclasts induced by M-CSF and RANKL in a concentration-dependent manner.

Next, to further investigate the potential therapeutic value of TAS05567 for autoimmune diseases, we evaluated its effects in representative rodent models of arthritis, collagen antibody-induced arthritis (CAIA) and collagen-induced arthritis (CIA). TAS05567 inhibited the development of arthritis based on clinical scores of CAIA or hind paw volume in CIA. Additionally, serum biomarker (MMP-3, IgG, and COMP) levels were significantly lower in the TAS05567 groups than in the vehicle group. In the experiment of rat CIA, we performed histopathologic examination of the left and right hind paws. TAS05567 significantly reduced inflammatory cell infiltration into the synovium and pannus formation and markedly ameliorated damage to cartilage and bone. At the same time, we monitored changes in body weight during treatment as an index of general toxicity and assessed red blood cell count and hemoglobin levels because anemia was observed in some patients during clinical trials of drugs with JAK2 inhibition. TAS05567 did not significantly reduce body weight, the red blood cell count or hemoglobin level compared with control rats. Furthermore, we examined whether TAS05567 could attenuate platelet count decreases in mice with thrombocytopenia induced by administration of an antiplatelet antibody, because Syk is profoundly

involved with the pathogenesis of ITP via the activation of FcγR. In mice injected with an anti-CD41 antibody, the platelet count decreased by more than 50% compared with sham mice. In this model, TAS05567 provided significant protection against anti-CD41 antibody–induced thrombocytopenia in a dose-dependent manner. We evaluated the therapeutic effects of TAS05567 on other indications, including type 1 allergic diseases as well as B-cell malignancies, using *in vitro* assay as well as preclinical animal models. Syk reportedly plays a crucial role in FcεR-mediated production of chemical mediators by mast cells. Therefore, we evaluated the inhibitory effects of TAS05567 on IgE-induced histamine release by RBL-2H3 cells. TAS05567 suppressed histamine release by IgE stimulation in a concentration-dependent manner. We next examined whether TAS05567 is a potent drug for treatment of B-cell malignancies, we confirmed cytotoxic activity of our compound toward diffuse large B-cell lymphoma (DLBCL) cells, which depend on chronic active BCR signaling for survival. TAS05567 reduced the cell viability of several DLBL cell lines in a concentration-dependent manner. Furthermore, to examine whether TAS05567 could suppress the type 1 allergic reactions *in vivo*, we used 2,4,6-trinitrophenol (TNP) -IgE transgenic mice. Administration of picryl chloride to the ears of the mice provoked ear swelling, which reached a peak 2 h after antigen challenge. TAS05567 strongly suppressed ear swelling from 1 to 4 h after

antigen challenge. Finally, the *in vivo* antitumor activity of TAS05567 was evaluated in SCID mice bearing SU-DHL-10 xenograft. TAS05567 significantly inhibited the tumor growth and decreased the levels of EGR2 mRNA and phosphorylation of BLNK in the tumor tissues, as compared with vehicle control.

We determined the pharmacologic profile of a novel selective Syk inhibitor, TAS05567, which potently inhibited BCR signaling, FcR-dependent cellular functions, osteoclast differentiation, and proliferation of DLBCL cells. After oral administration, TAS05567 not only was ameliorated symptoms in animal models of several inflammatory diseases, but also suppressed tumor growth in the mouse xenograft model using DLBCL cells. Notably, TAS05567 showed less off-target activity, such as VEGFR2 and JAK2 inhibition, than R406, suggesting that the efficacy/toxicity profiles of our Syk inhibitor and fostamatinib differ. Our data suggest that TAS05567 would be an efficacious novel treatment for inflammatory diseases as well as B-cell malignancies.

General Introduction

Uncontrolled immune responses that attack either self-tissues and/or innocuous environment antigens lead to autoimmune diseases and allergic conditions.

Epidemiological researches provide evidence that autoimmune diseases prevalence has grown throughout the last century, mostly in the western world [1-3]. RA is a representative autoimmune disease characterized by systemic inflammatory disorder affecting approximately 1% of the world's population that causes chronic synovial inflammation and joint destruction [4]. Disease-modifying anti-rheumatic drugs (DMARDs) with potential immunosuppressant activity, such as methotorexate, sulfasalazine, and cyclosporine, are available for the management of RA, but an American College of Rheumatology (ACR) 50 response (based on standard criteria for assessing RA symptoms) is only achieved in approximately half of all patients and an ACR 70 response is attained by a minority [5]. Although biological drugs, including anti-tumor necrosis factor (TNF)-α antibody and anti-interleukin (IL)- 6 antibody, and Janus kinase (JAK) inhibitors have proved effective for active RA in recent clinical trials, there are still unmet clinical needs because these agents are associated with

antibody production and adverse events, such as an increased risk of infection or malignancy [6-8]. Therefore, new therapies with stronger efficacy and a better safety profile are needed for RA patients who have severe symptoms or are refractory to treatment with conventional DMARDs or biological agents.

Autoimmune diseases, including RA, are caused by aberrant immune responses that generally involve production of autoantibodies against auto-antigens [9, 10]. Various immune cells, including B-cells, monocytes, macrophages, neutrophils, and dendritic cells, express receptors for the Fc portion of immunoglobulins (Igs) [11, 12]. During the chronic inflammatory process of RA, immune complexes (ICs) formed by autoantigens and autoantibodies are deposited in synovial tissues and activate effector cells through the Fc gamma receptor (FcγR), leading to cytokine production, synovial inflammation, and joint damage [13]. The importance of autoantibodies in the pathogenesis of RA is also supported by current treatments, e.g., suppression of pathogenic antibody production by depleting B cells with rituximab has been shown to be effective for RA [14, 15]. In addition, passive transfer of antibodies targeting type II collagen produces pathologic joint changes in mice resembling those in human RA [16]. Importantly, mice lacking FcγR do not develop inflammatory joint changes or symptoms after antibody transfer [17, 18], which suggests that targeting the FcγR signaling pathway is a potential

therapeutic strategy for preventing the progression of RA.

ITP is an autoimmune bleeding disorder caused by the improper functioning or destruction of platelets. Incidence of ITP has been estimated to be from 0.46 to 12.5/100,000 person-years in children and from 1.6 to 3.9/100,000 person-years in adults [19]. There is an estimate of approximately 3,000 new cases of this disorder in Japan every year [20]. Since 1974, ITP has been specified as an intractable disease in Japan, and some patients have received public financial support from the national governments. Circulating platelets are opsonized by platelet-specific autoantibodies, resulting in their premature destruction by macrophages. [21]. Many ITP patients show a good response to current treatments, such as steroids and splenectomy, but a small group remains at risk of life-threatening cerebral hemorrhage due to a persistent low platelet count [22, 23]. Similar to RA, ICs have been implicated in the pathogenesis of ITP because intravenous immunoglobulin (IVIg) targeting FcγR is effective in patients with ITP [24], and because injection of antibodies against platelet surface antigen to mice decreases the platelet count like the pathogenesis of human ITP [25]. Based on these findings, the FcγR signaling cascade has become an attractive target for treatment of ITP.

Other types of inflammatory diseases, such as allergic diseases, are caused by an

ineffective tolerogenic immune response towards allergens. Similar to autoimmune diseases, the prevalence of allergic diseases are increasing worldwide, particularly in low and middle income countries [26]. Although therapies for allergic diseases have improved over the years with the introduction of agents directed against the inflammatory processes, those therapies have remained, for the most part, non-curative [27]. In particular, type 1 allergic diseases such as urticaria, asthma, and allergic rhinitis are predominantly caused and exacerbated by IgE-mediated allergic reactions [28, 29]. Antigen-induced cross linking of IgE-bound FcεRI leads to activation of mast cells and basophils followed by release of a variety of biochemical mediators, such as histamine and arachidonic acid metabolites [30]. Importantly, FcεRI-deficient mice fail to develop increased inflammatory responses even after repeated exposure to antigen [31]. Omalizumab, a monoclonal antibody that inhibits the interaction between IgE and FcεRI, has been shown effective in patients with severe allergic asthma [32]. Therefore, targeting the FcεRI signaling pathway is a promising therapeutic option for type 1 allergic diseases.

Spleen tyrosine kinase (Syk) is a 72 kDa non-receptor cytoplasmic tyrosine kinase that is primarily expressed by cells of hematopoietic lineage [33]. Syk acts downstream of immunoreceptor tyrosine-based activation motif–coupled receptors, including the

B-cell receptor (BCR), FcRs, and integrin signaling, and influences diverse biological events, such as cytokine production, degranulation, differentiation, and adhesion [34, 35], suggesting that Syk is profoundly involved in the development of autoimmune and allergic diseases. For example, direct injection of Syk siRNA into the limb joints or genetic deficiency of Syk in hematopoietic cells prevents joint swelling and bone erosion in models of type II collagen autoantibody-induced arthritis [36, 37]. In addition, Syk-deficient macrophages show severely impaired phagocytosis of IgG-opsonized particles in response to FcγR activation [38]. Besides its crucial role in inflammation, Syk contributes directly to bone resorption in RA, because Syk kinase activity regulates RANK, which is the receptor for the RANKL signaling pathway that is essential for differentiation and activation of osteoclasts [39]. Regarding the relationship with allergic reactions, Syk-deficient mast cells fail to degranulate and secrete mediators when stimulated through FcεRI [40]. Considering its biological actions and its association with the pathogenesis of autoimmune and allergic diseases, pharmacologic inhibition of Syk represents a potential therapeutic intervention option for patients with these diseases.

In another aspect, Syk is also a key factor in the pathogenesis of B-cell malignancies because chronic activation of the BCR pathway is crucial for proliferation and survival

of malignant B cells [41]. Actually, Syk protein is activated in approximately half of primary human diffuse large B-cell lymphoma (DLBCL) tissues, the most common non-Hodgkin's lymphoma that develops from the B-cells in the lymphatic system [42]. DLBCL is known to be aggressive, with poor prognosis without adequate therapy. While 5-year survival rates in the first-line setting range from 60% to 70%, 40%-50% of patients remain refractory to the therapy [43]. Therefore, new therapeutic drugs are needed to improve survival. Of note, genetic knock down of Syk causes cell-cycle arrest and decelerates the proliferation of the Syk-positive DLBCL cells [42]. From these findings, Syk inhibitors have potential as therapeutic drugs for not only autoimmune and allergic diseases but also B cell malignancies including DLBCL (See below figure).

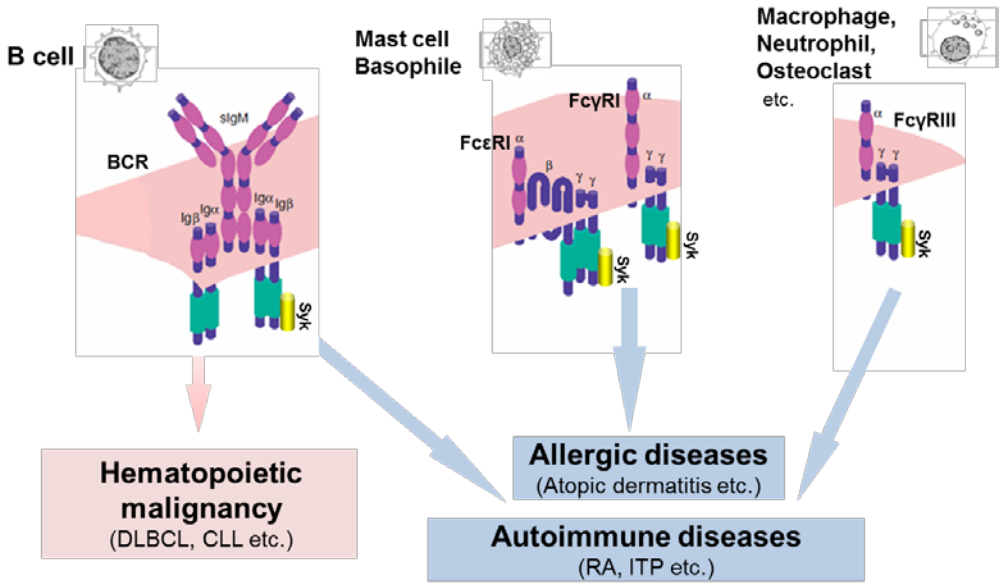

Indeed, several ATP-competitive Syk inhibitors, notably fostamatinib (Rigel

Pharmaceuticals), have already been evaluated in clinical trials performed in patients with autoimmune diseases, including RA and ITP [44]. Even though fostamatinib was efficacious against chronic refractory ITP [45], it is unclear whether inhibition of Syk activity specifically contributed to the clinical response and adverse events observed in the clinical trials, as this drug inhibits several kinases, including vascular endothelial growth factor receptor (VEGFR) 2 and Janus kinase (JAK) 2 [46, 47]. Another Syk inhibitor (GS-9973, entospletinib, Gilead Sciences) has been developed for the treatment of leukemia including DLBCL, but it inhibits multiple protein kinases within 100-fold of its inhibitory concentration 50 (IC50) value for Syk [48]. These findings suggest that novel Syk inhibitors with different activity profiles from the above-mentioned inhibitors are required to provide new therapeutic options. Against this background, we tried to identify a novel, potent, and selective orally available Syk inhibitor. We synthesized a series of potent and highly selective ATP-competitive novel inhibitors of Syk. Investigation of structure-activity relationships led to identification of TAS05567 as a lead compound.

In this study, the pharmacological properties and utility of TAS05567, a novel Syk inhibitor, were investigated for the purpose of clarifying the difference with the preceding Syk inhibitors. In Chapter 1, we employed biochemical assays and cell-based

assays to characterize the basic features of TAS05567. In addition, we performed pharmacodynamics analyses to predict its *in vivo* activity using specimens from animals. Moreover, we examined the therapeutic potential of TAS05567 for autoimmune diseases using two types of rodent arthritis models as well as a passive antibody-induced ITP model. In Chapter 2, to assess the therapeutic potential of TAS05567 against allergic diseases and B-cell malignancies, we first evaluated the inhibitory activity of TAS05567 against histamine release and cell proliferation of cancer cells. Furthermore, we determined whether TAS05567 could suppress type I allergic reactions using IgE-mediated dermatitis model. Finally, we evaluated the antitumor activity of TAS05567 in subcutaneous xenograft tumors of human DLBLC cells.

Chapter 1

Identification of pharmacological properties of TAS05567 and its therapeutic potency against autoimmune diseases

1.1 Introduction

RA is a complex systemic inflammatory autoimmune disease characterized by excessive and chronic inflammation in joints, associated with synovial hyperplasia and with cartilage and bone destruction [49, 50]. Though activation of T cells can produce several proinflammatory cytokines, activation of B cells, autoantibody production, immune complex formation, and its deposition within the synovium are also profoundly involved in the pathogenesis of this disease [51, 52]. ITP is also an autoimmune disease in which autoantibodies against antigens on platelets result in the opsonization and phagocytosis of platelets by macrophages [21].

Syk tyrosine kinase is essential for signaling from the BCR as well as FcR, and thus profoundly associated with autoantibody responses [34, 35]. Currently, several small molecule inhibitors targeted towards activity of Syk kinase have been developed for patients with immune-mediated inflammatory diseases [53]. Fostamatinib, a representative inhibitor of Syk, shows inhibitory effects on activity of Syk kinase in an

enzymatic assay and Ig-mediated signaling cascades as well as proinflammatory cytokine production in cell-based assays [46]. R406, an active metabolite of Fostamatinib, also exhibits significant efficacy in some preclinical models of autoimmune diseases, such as collagen-induced arthritis (CIA) and anti-CD41 antibody-induced thrombocytopenia [45, 54]. Of note, Fostamatinib produces clinically significant responses in patients with chronic ITP who had relapsed or not responded to splenectomy and thrombopoietic agents [55]. The Food and Drug Administration (FDA) has approved fostamatinib as a second-line treatment for patients with chronic ITP following insufficient response to a previous therapy, based on the results of clinical trials. Fostamatinib also provides some clinical benefits to patients with active RA receiving methotrexate treatment in a 3-month, placebo-controlled trial [56]. However, it is unclear whether inhibition of Syk activity specifically contributed to reduction of symptoms in patients with autoimmune diseases, because Fostamatinib inhibits several other kinases, including VEGFR2 and JAK2, which are associated with the potential risk of hypertension and anemia [46, 47, 57, 58]. Indeed, hypertension was more frequent in the Fostamatinib group than in the placebo group during clinical trials for RA, and also anemia was observed in the lymphoma patients treated with this drug [59, 60]. Moreover, adverse events such as elevation in transaminase enzymes and increase

in incidence of infection have been reported in patients receiving fostamatinib, which may be related to off-target inhibition of this drug [61]. Since these adverse events may limit the use of fostamatinib in the clinical setting, Syk inhibitors with a different profile from fastamatinib are expected to produce a benefit to patients with autoimmune diseases.

In this chapter, we first assessed the potency and selectivity of TAS05567 by a wide range of biochemical assays as well as Ig-mediated intracellular signaling pathway analyses by using R406 as a comparator. In addition, Syk-mediated cellular functions, such as production of proinflammatory cytokines associated with the pathogenesis of RA and differentiation of osteoclasts, were evaluated by *in vitro* experiments. Moreover, we determined the plasma protein binding of TAS05567 using mouse, rat, and human plasma to investigate whether there were species differences in plasma protein binding ratio of it. We further examined pharmacodynamics and pharmacokinetics of TAS05567 using mice and rats to determine dosage of our compound for *in vivo* experiments. In *in vivo* studies, we evaluated the effects of TAS05567 on synovial inflammation, bone destruction, and serum markers associated with the pathogenesis of RA using CAIA and CIA that have been recognized as representative models of RA. Regarding the tolerability and safety of TAS05567, body weight changes and anemia risk were

assessed in a study using the rat CIA model. Finally, to investigate the therapeutic potential of TAS05567 in ITP, we utilized anti-CD41 antibody-induced thrombocytopenia model, which is based on a self-antigen that is highly relevant to the human disorder [25].

1.2 Materials and Methods

1.2.1 Reagents

TAS05567, 3-(((3R, 4R)-3-aminotetrahydro-2H-pyran-4-yl) amino)-5-((2-(tert-butyl)-7-methyl-2H-indazol-5-yl) amino)-1, 2, 4-triazine-6-carboxamide, was designed and synthesized by Taiho Pharmaceutical Co., Ltd. R406 was purchased from Santa Cruz Biotechnology, Inc. (Santa Cruz, CA, USA). Prednisolone was purchased from Sigma-Aldrich, Co. (St. Louis, MO, USA). Polyglobin® N 10% (IVIg) was obtained from Japan Blood Products Organization (Tokyo, Japan). For in vitro experiments, TAS05567 and R406 were dissolved in dimethyl sulfoxide. R788, a prodrug of R406, was purchased from Medchemexpress LLC (Princeton, NJ, USA).

1.2.2 Biochemical Assays

The Off-chip Mobility Shift Assay was employed for measurement of kinase inhibitory activity. Recombinant FLT3, JAK2, VEGFR2, Syk, and RET (Carna Biosciences, Kobe, Japan) were used for activity assays in 20 mM HEPES buffer (pH 7.5) with 0.01% Triton X-100 and 2 mM dithiothreitol. Each recombinant kinase was reacted with the appropriate peptide substrate in the presence of ATP (at room temperature (RT), followed by measurement of the product ratio using the LabChipTM system (PerkinElmer, Waltham, MA, USA). The selectivity of TAS05567 was assessed

with a panel of 192 kinases using the Profiler Pro kit (PerkinElmer) according to the manufacturer's instructions. The plates were read using a LabChip EZ Reader (PerkinElmer).

1.2.3 Off-target receptor binding assays

TAS05567 was tested at 10 μM for orthosteric radioligand displacement against a panel of 68 primary molecular targets, such as G-protein-coupled receptors, ion channels, and transporters, to characterize its specificity using the LeadPrifilingScreen commercial assay (Eurofins Panlabs Taiwan, Taipei, Taiwan). Results that show an inhibition or stimulation >50% were considered to represent significant effects on the test compound.

1.2.4 Detection of B-cell Linker Protein (BLNK), Phospholipase C (PLC) γ2, and Extracellular Signal-regulated Kinase (ERK) Phosphorylation (Ramos cells)

A human B cell lymphoma cell line (Ramos, ATCC CRL-1596) was purchased from the American Type Culture Collection (Manassas, VA, USA) and maintained in Roswell Park Memorial Institute (RPMI) -1640 medium (Sigma-Aldrich) containing 10% fetal bovine serum (FBS). Ramos cells (1×10^5 cells/100 μl) were pretreated with test compounds, followed by stimulation with goat F(ab')2 anti-human IgM (5 μg/ml; Southern Biotech, Birmingham, AL, USA) for 5 min at 37°C. The cells were then fixed

in Phosflow fix buffer I (BD Biosciences, San Jose, CA, USA) for 10 min at 37°C and permeabilized in Phosflow perm buffer III (BD Biosciences) for 30 min on ice. After membrane permeabilization, the cells were washed in staining buffer (FBS) (BD Biosciences) and resuspended and incubated for 1 h at RT in the same buffer containing phycoerythrin (PE) -labeled mouse anti-BLNK (pY84) (clone J117-1278), Alexa Fluor 647–labeled mouse anti-PLCγ2 (pY759) (clone K86-689.37), and Alexa Fluor 488–labeled mouse anti-ERK1/2 (pT202/pY204) (clone 20A) (all from BD Biosciences). Subsequently, the cells were washed and resuspended in staining buffer (FBS). Phosphorylation of BLNK, PLCγ2, or ERK1/2 induced by anti-IgM antibody was quantified using a flow cytometer (BD Biosciences).

1.2.5 FcγR- and Lipopolysaccharide-mediated Tumor Necrosis Factor (TNF)-α Production Assay

To assess FcγR-mediated TNF-α production, an Immulon 4 HBX 96-well plate (Thermo Fisher Scientific, Waltham, MA, USA) was coated overnight at 4°C with 100 μg/ml of purified human IgG (R&D Systems, Minneapolis, MN, USA), and was washed with phosphate-buffered saline (PBS) (−) (Wako Pure Chemicals, Osaka, Japan). Next, THP-1 cells (ATCC TIB-202) were seeded into the IgG-coated plate at a density of 2×10^6 cells /ml and incubated for 4 h at 37°C. To measure lipopolysaccharide

(LPS)-mediated TNF production, THP-1 cells were seeded at the same density and pretreated with TAS05567 for 1 h, followed by stimulation with LPS (1 μg/ml, Sigma-Aldrich) for 24 h at 37°C. The TNF-α level in the supernatant was determined by ELISA (R&D Systems).

1.2.6 FcγRI-mediated Phagocytosis Assay

Phagocytic ability was evaluated by measuring the amount of uptake of latex beads coated with FITC-labeled IgG into cells by a phagocytosis assay kit (Cayman Chemical, Ann Arbor, MI, USA) according to the instruction manual. Briefly, RAW264.7 cells (ATCC TIB-71) were seeded in 6-well plates (1×10^6 cells/well) in DMEM containing 5% FBS overnight at 37°C to allow adherence to the plate. On the next day, the latex beads were added directly to the culture medium at a dilution of 1:500 and incubated at 37°C for 4 h. The cells were collected and analyzed by flow cytometry (BD Biosciences).

1.2.7 Stimulation with an Inflammasome Activator

THP-1 cells were differentiated by incubation with 0.2 μM PMA (Sigma-Aldrich) for 3 days at 37°C and were seeded overnight at 37°C in a 96-well plate (2×10^4 cells/well) in RPMI-1640 containing 10% FBS to allow adhesion. On the next day, the cells were primed with LPS (1 μg/ml) in serum-free RPMI-1640 for 3 h and then pretreated with

TAS05567 for another 1 h at 37°C. Subsequently, the cells were stimulated with Imject™ Alum Adjuvant (30 μg/ml; Thermo Fisher Scientific) for 9 h at 37°C, and the IL-1β level in the supernatant was determined by ELISA (R&D systems).

1.2.8 Differentiation of Osteoclasts

Primary human osteoclast precursor cells (Lonza, Walkersville, MD, USA) were cultured according to the manufacturer's instructions. Next, 33 ng/ml of macrophage colony-stimulation factor (M-CSF) and 66 ng/ml of RANKL (Lonza) were added to the culture medium (OCP BulletKit® Lonza; containing 10% FBS). After differentiation of osteoclasts, staining was performed on day 5 using a tartrate-resistant acid phosphate (TRAP) staining kit (Cosmo Bio, Tokyo, Japan), and the number of mature osteoclasts (TRAP-positive multinucleated cells >100 μm in diameter) per well was determined by manual counting.

1.2.9 Experimental Animals

All animal experiments were approved by the Animal Experiments Ethics Committee of Taiho Pharmaceutical Co., Ltd. The animals used for the present study were BALB/c (female and male) mice, male DBA1/J mice, female C57BL/6J mice, female Lewis rats, and male Sprague-Dawley rats from Charles River Laboratories Japan (Yokohama, All animals were housed in cages and maintained under a 12-h light/dark cycle with water

and food supplied ad libitum. During the experimental period, animals were observed to assess activity, feeding, and signs of pain in accordance with the established protocol. For administration, TAS05567 was dissolved in a solution of 0.5% hydroxypropyl methyl cellulose (Shinetsu Chemical, Tokyo, Japan) with 0.1 N HCl, and prednisolone was suspended in a solution of 0.5% HPMC without HCl. R788, a prodrug of R406, was used for *in vivo* experiments. R788 was dissolved in 0.1% carboxymethylcellulose, 0.1% methylparaben–0.02% propylparaben–99.78% water, according to a previous report [45]. IVIg (500 mg/50 ml) was administered by intravenous injection at a volume of 10 ml/kg.

1.2.10 BLNK Phosphorylation in Whole Blood

For analysis of phosphor-BLNK in mice, blood samples were collected into heparinized tubes from non-immunized male BALB/c mice (7-9 weeks old) and then aliquots of the blood (80 µl) were transferred to test tubes. TAS05567 was added for 30 min at the indicated concentrations prior to stimulation with goat anti-mouse IgD (1:100, Thermo Fisher Scientific) for 10 min at 37°C, and stimulation was suppressed by addition of Lyse/Fix Buffer (BD Biosciences) according to the manufacturer’s protocol. Fixed cells were incubated overnight at 4°C with PerCP-conjugated anti-mouse CD45R/B220 antibody (Clone RA3-6B2) (BD Biosciences) and PE-conjugated anti-BLNK antibody

(pY84) (clone J117-1278). For the experiment in rats, blood samples were collected into heparinized tubes from male Sprague-Dawley rats (7-8 weeks old) and then aliquots (180 µl) of the blood were transferred to test tubes. TAS05567 was added for 1 h prior to stimulation with anti-rat IgD (20 µg/ml, Thermo Fisher Scientific), and stimulation was suppressed by addition of Lyse/Fix Buffer (BD Biosciences). Fixed cells were incubated for 1 h at RT with FITC-conjugated ant-rat CD45RA antibody (clone OX-33) (BD Biosciences) and PE-conjugated anti-BLNK antibody (pY84) (clone J117-1278). Phosphorylation of BLNK induced by anti-IgD antibody was quantified using a flow cytometer (BD Biosciences).

1.2.11 Plasma protein binding

TAS05567 (in 50:50 acetonitrile/water) was tested at a final concentration of 1 µM in mouse, rat（Charles River Laboratories Japan, Yokohama, Japan), and human plasma (Biopredic, Rennes, France). An aliquot of 150 µl plasma containing TAS05567 was in donor side of the well of 96-well micro-equilibrium dialysis device (HTD 96b, HTDialysis, CT, USA). An aliquot of 150 µl PBS was added in reservoir side of the same device. The plate containing plasma and buffer was equilibrated at 37°C for 6 h, with constant shaking at 80 rpm on an orbital shaker. Samples were collected from respective sides after 6 h. All samples were centrifuged at 850*g* for 5 min at 4°C, and

then were analyzed by liquid chromatography–tandem mass spectrometry. Data are presented as mean ± SD (n = 3).

1.2.12 BLNK Phosphorylation in Whole Blood

For analysis of phosphor-BLNK in mice, blood samples were collected into heparinized tubes from non-immunized male BALB/c mice (7-9 weeks old), and then aliquots of the blood (80 µl) were transferred to test tubes. TAS05567 was added and incubated for 30 min at the indicated concentrations prior to stimulation with goat anti-mouse IgD (1:100, Thermo Fisher Scientific) for 10 min at 37°C. Stimulation was suppressed by addition of Lyse/Fix Buffer (BD Biosciences) according to the manufacturer's protocol. Fixed cells were incubated overnight at 4°C with PerCP-conjugated anti-mouse CD45R/B220 antibody (Clone RA3-6B2) (BD Biosciences) and PE-conjugated anti-BLNK antibody (pY84) (clone J117-1278).

For the experiment male Sprague-Dawley rats (7-8 weeks old), blood samples were collected into heparinized tubes, and then aliquots (180 µl) of the blood were transferred to test tubes. TAS05567 was added and incubated for 1 h prior to stimulation with anti-rat IgD (20 µg/ml, Thermo Fisher Scientific), and stimulation was suppressed by addition of Lyse/Fix Buffer (BD Biosciences). Fixed cells were incubated for 1 h at RT with FITC-conjugated ant-rat CD45RA antibody (clone OX-33) (BD Biosciences) and

PE-conjugated anti-BLNK antibody (pY84) (clone J117-1278). Phosphorylation of BLNK induced by anti-IgD antibody was quantified using a flow cytometer (BD Biosciences).

1.2.13 Pharmacokinetics

TAS05567 was orally administered to male BALB/c mice at 10 mg/kg (dosing volume of 10 ml/kg), and blood samples were collected with a heparinized syringe at 0.5, 1, 2, 4, and 6 h after administration. In addition, TAS05567 was orally administered to male Sprague-Dawley rats at 10 or 25 mg/kg (dosing volume of 10 ml/kg), and blood samples were collected at 1, 2, 4, 8, and 24 h after administration. The blood samples were centrifuged at 10,000*g* for 5 min at 4°C to obtain plasma, which was stored at −80°C until use. Plasma drug concentrations were determined by liquid chromatography–tandem mass spectrometry.

1.2.14 Mouse Model of Collagen Antibody-induced Arthritis (CAIA)

On day 0, female BALB/c mice (7-8 weeks old) were intravenously injected with 2 mg of an arthritogenic cocktail containing 5 monoclonal antibodies (Chondrex, Redmond, WA, USA), followed by intraperitoneal injection of LPS (100 μg) on day 4. Mice were randomly divided into vehicle, prednisolone, and TAS05567 groups, and the test drugs were administered daily from day 0. Arthritis was assessed on days 0, 3, 6,

and 9 by using the following clinical scoring system: 0, normal paw; 1, one swollen digit; 2, more than one swollen digit; 3, swelling of the entire paw; 4, swelling of the paw and all digits. The maximum possible score was 16 (4 x 4 paws). Serum MMP-3 levels were determined by ELISA (R&D Systems).

1.2.15 Mouse Model of Collagen-induced Arthritis (CIA)

On day -21, male DBA/1 mice (7 weeks old) were anesthetized with isoflurane and 0.1 ml of complete Freund's adjuvant (BD Biosciences) containing 2 mg/ml bovine type II collagen (Collagen Research Center, Tokyo, Japan) was injected at one site on the back. For booster immunization, the mice were injected with 0.1 ml of incomplete Freund's adjuvant (BD Biosciences) containing 2 mg/ml bovine type II collagen at one site on the tail under anesthesia on day 0. Oral administration of TAS05567 was initiated on day 0 of the study and continued to day 14. Arthritis was assessed on days 0, 4, 7, 10, and 14 by the same criteria as those used for grading CAIA. The serum level of anti-bovine type II collagen IgG was determined by ELISA (Chondrex).

1.2.16 Rat Model of Established CIA

On day -14, female Lewis rats (7 weeks old) were anesthetized with isoflurane and injected with incomplete Freund's adjuvant (BD Biosciences) containing 2 mg/ml bovine type II collagen at nine sites on the back and two on the tail (0.1 ml per site),

followed by booster injection at 2 sites on the tail (0.1 ml per site) on day -7. Oral administration of TAS05567 and prednisolone was initiated on day 1 of the study and continued to day 14. The volume of both hind paws was measured on days 1, 7, and 14 by water displacement using a plethysmometer for rats (MK-101P; Muromachi Kikai, Tokyo, Japan). Body weight was also measured every day to monitor toxicity. At the end of the experiment, blood samples were collected for measurement of the red blood cell count and hemoglobin using a hematology autoanalyzer (Sysmex XT-2000iV; Sysmex, Kobe, Japan). In addition, the serum level of cartilage oligomeric matrix protein (COMP) was determined by enzyme-linked immunosorbent assay with a kit from Immunodiagnostic Systems (Boldon, UK) and both hind paws were harvested for histopathological examination.

1.2.17 Histopathological examination

Rat hind limbs were decalcified in formalin with 10% formic acid (Wako Pure Chemical Industries, Tokyo, Japan) and embedded in paraffin blocks, which were cut into sections, stained with hematoxylin-eosin (H&E), and randomly selected for microscopic examination. Then the hind limb joints were evaluated by assigning a histopathological score for each of four pathological changes (inflammation, pannus, cartilage damage, and bone damage) on a 5-grade scale from 0 to 4 (0 = normal and 4 =

the most severe changes). The histopathological scores for each pathological change were summed for both hind limbs to calculate the total score per animal (maximum: 8 points).

1.2.18 Mouse Model of Immune Thrombocytopenia

Female C57BL/6J mice (8 weeks old) received TAS05567 orally on days 1 and 2. In the IVIg group, mice were injected intravenously with IVIg (1 g/kg) on day 1, followed by intravenous injection of 2 μg of anti-CD41 antibody (clone MWReg30, Thermo Fisher Scientific) in 0.2 ml of PBS on day 2. On day 3, 200 μL of peripheral blood was collected in a K_2EDTA-coated Microtainer tube (BD, Franklin Lakes, NJ, USA), and the platelet count was determined with a Sysmex XT-2000iV hematology autoanalyzer (Sysmex).

1.2.19 Statistical Analysis

Statistical analysis and determination of half-maximal inhibitory concentration (IC50) values were performed with EXSUS software, version 8.0.0 (CAC Exicare, Tokyo, Japan). Results are reported as the mean ± standard deviation (SD) for *in vitro* experiments or the mean ± standard error of the mean (SEM) for *in vivo* experiments.

Evaluation of the efficacy of TAS05567 in the rodent inflammation models was performed by using Dunnet's test, while the statistical significance of differences in

histopathological scores was assessed with Steel's test. In all analyses, $P<0.05$ was considered to indicate statistical significance.

1.3 Results

1.3.1 Potency and Selectivity of TAS05567

The chemical structure of TAS05567 is shown in Figure 1A. TAS05567 potently inhibited the activity of Syk, showing an average IC50 (mean ± SD) of 0.37 ± 0.029 nM in enzymatic assays in the presence of ATP concentration close to the Km value. TAS05567 was more potent than R406, exhibiting an average IC50 of 13 ± 0.26 nM under the same condition. The specificity of TAS05567 for Syk was determined at 50 nM (approximately 140 times the IC50 value) using a panel of 192 kinases. In these analyses, TAS05567 only showed >70% inhibition of Syk and 4 other kinases (Figure 1B and Table 1). In comparison, R406 at 500 nM (approximately 40 times its IC50 for Syk) showed >70% inhibition of 43 of the 192 kinases. During clinical trials of fostamatinib in patients with RA, adverse events such as hypertension, neutropenia, and anemia were considered to be related to inhibition of VEGFR2 and JAK2 [46, 47]. Accordingly, the IC50 values of TAS05567 and R406 were determined for 4 selected kinases, including VEGFR2 and JAK2. Whereas TAS05567 showed at least 10-fold selectivity for Syk over the 4 kinases, R406 showed equal or greater efficacy against these kinases (Table 2). In addition, the enzymatic assays of Syk as well as the selected 4 kinases were performed at 1 mM ATP to approximate cellular concentrations. In the

presence of a physiologically relevant ATP concentration, TAS05567 inhibited Syk activity with IC50 of 1.5 ± 0.40 nM, but much less activity against the 4 kinases (Table 2). Furthermore, the selectivity of TAS05567 for non-kinases targets was evaluated using a Panlabs Lead Profiling screen. In this assay, TAS05567 at 10 μM only inhibited 1 of the 68 targets tested (inhibition of radioligand binding >50%) (Table 3).

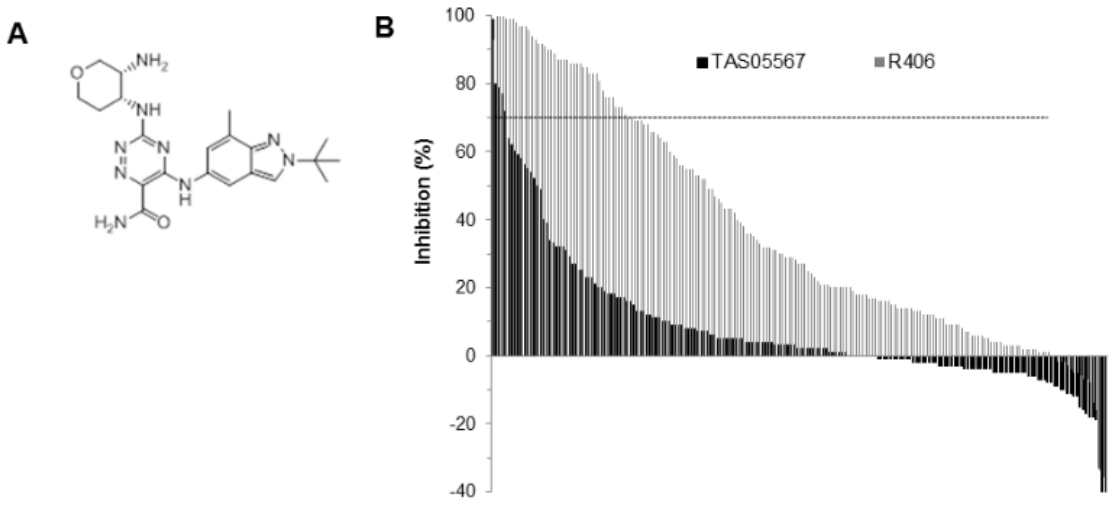

Figure 1. Selectivity of TAS05567 and R406 against a panel of 192 kinases.

(A) Chemical structure of TAS05567. (B) TAS05567 and R406 were evaluated using the Profiler Pro kit. Values represent percent inhibition at 50 nM (TAS05567; approximately 140-fold the IC50 value of Syk kinase) and at 500 nM (R406; approximately 40-fold the IC50 value of Syk kinase). Inhibitory activity of 70% is shown as a dashed line.

Table 1. Selectivity profile of TAS05567 and R406 for kinase from the Profiler Pro Kit.

Enzyme TAS05567

Enzyme	TAS05567 % inh at 50 nM	R406 % inh at 500 nM	Enzyme	TAS05567 % inh at 50 nM	R406 % inh at 500 nM	Enzyme	TAS05567 % inh at 50 nM	R406 % inh at 500 nM
ABL	1	20	EPHB3	2	25	NuaK1	31	87
Abl(H396P)	-11	-3	EPHB4	2	21	p38a	2	27
Abl(Q252H)	-17	-7	Erk1	-1	14	p38alpha/SAPK2a (T106M)	-11	-4
Abl(T315I)	-55	-36	Erk2	3	30	p38-beta2	-2	13
ABL1(E255K)	-15	-6	Fer	55	96	p38-delta	4	36
ABL1(G250E)	-16	-7	FES	2	27	p38-gamma	-1	14
ABL1(Y253F)	-12	-5	FGFR1	-3	11	p70S6K	0	17
AKT1	13	68	FGFR1 (V561M)	-19	-16	PAK2	1	20
AKT2	0	17	FGFR2	2	24	PAK3	9	56
AKT3	-1	14	FGFR2(N549H)	-18	-8	PAK4	77	100
ALK	62	99	FGFR3	-3	9	PAK5 (PAK7)	80	100
AMPK	3	29	FGFR3 [K650E]	-18	-14	PASK	-5	2
AMPK-alpha2/beta1/gamma1	0	17	FGFR4	-5	3	PDGFR beta	-1	15
Arg	-3	9	FGR	-7	1	PDGFR_alpha	4	32
AurA	10	63	FLT1	-5	4	PDGFRA (D842V)	-9	0
AurB	2	23	FLT3	17	73	PDGFR-alpha(V561D)	-10	-2
AurC	-5	4	Flt3(D835Y)	-8	1	PhKg1	-2	12
AXL	1	20	FLT4	4	33	PhKg2	-3	11
BLK	27	86	FMS	-2	13	PIM1	-4	6
BMX	11	65	FRK	23	83	PIM2	56	97

BRSK1	-4	7	FYN	34	90	PIM3	0	19
BRSK2	-1	14	GCK	52	93	PKA	10	60
BTK	25	85	GSK3-alpha	8	53	PKC-alpha	27	86
CaMK1a	-5	4	GSK3b	9	58	PKCb2	-5	3
CamK1d	-2	12	Hck	5	46	PKC-beta1	18	73
CAMK2	0	18	HER4	4	31	PKC-delta	-3	9
CaMK2a	3	29	HGK	6	49	PKC-epsilon	7	52
CAMK4	-2	12	HIPK1	3	29	PKC-eta	8	55
CaMKII_beta	-6	2	HIPK2	-1	14	PKC-gamma	19	76
CaMKII_gamma	17	73	IGF1R	33	89	PKC-theta	23	83
Casein kinase 1g2	-1	16	IKBKE (IKK epsilon)	23	85	PKCz	-2	12
CDK1/Cycline B1	-5	3	IKK-beta	60	98	PKD1	-1	16
CDK2	5	43	INSR	32	87	PKD2	12	68
CDK3	-5	3	IRAK4	21	83	PKD3	-4	5
CDK5/p25	-4	4	ITK	5	45	PKG1-beta	0	18
CHK1	12	66	JAK2	79	100	PKGa	2	21
CHK2	17	71	VEGFR2	4	32	PRAK	10	63
CK1d	0	18	KIT	-7	1	PRKCI (PKC-iota)	1	20
CK1-epsilon	-1	16	KIT[T670I]	-74	-45	PRKX	1	20
CK1g3 (CSNK1G3)	-3	8	LCK	18	76	PYK2	29	86
CK1-gamma1	-1	16	LOK	59	97	RET	49	92
CLK2	1	20	LTK	18	76	Ret (V804L)	-12	-5
c-Raf	-1	15	LYN	40	91	RET Y791F	-9	-2
CSNK1A1	-2	11	LYNB	50	92	ROCK1	15	69
c-TAK1	-7	1	MAPKAPK2	9	59	ROCK2	25	86
DAPK1	4	36	MAPKAPK3	7	52	ROS (ROS1)	54	94
DCAMKL1	-4	6	MARK1	4	35	RSK1	3	28
DCAMKL2	-6	2	MARK2	-3	9	RSK2	3	31
DDR2	-6	2	MARK4	8	55	RSK3	9	56
DYRK1a	-5	3	MELK	-2	13	RSK4	4	34

DYRK1B	5	40	Mer	32	87	SGK1	8	55
DYRK3	0	20	MET	5	43	SGK2	6	47
DYRK4	2	27	MET M1250T	-10	-2	SGK3	11	64
EGFR	-3	9	MINK	16	70	SRC	39	90
EGFR (ErbB1) T790M L858R	-8	0	MNK1 (MKNK1)	16	70	SRM (SRMS)	-4	6
EGFR(T790M)	-33	-34	MSK1	0	18	SYK	99	93
EPHA1	11	66	MSK2	-5	3	TEC	-5	2
EPHA2	5	39	MST1	64	99	TRKC (NTRK3)	13	69
EPHA3	7	49	MST1R	2	21	TSSK1	58	97
EPHA4	2	22	MST2	20	78	TSSK2	20	81
EPHA5	5	38	MST3 (STK24)	3	30	TXK	-4	6
EPHA8	5	42	NEK1	-4	5	TYRO3	7	53
EPHB1	4	32	NEK2	-4	7	Yes	32	87
EPHB2	5	43	NTRK2 (TRKB)	13	69	ZIPK (DAPK3)	72	99

Table 2. Biochemical IC50 values for TAS05567 and R406 against 5 kinases.

Kinase	ATP (μM)	IC50 (nM)		ATP (μM)	IC50 (nM)	
		TAS05567	R406		TAS05567	R406
Syk	26	0.37 ± 0.029	13 ± 0.26	1000	1.5 ± 0.40	67 ± 14
FLT3	94	10	< 0.30	1000	39	0.56
JAK2	13	4.8	0.86	1000	160	25
VEGFR2	74	600	9.8	1000	2600	42
RET	7.5	29	2.8	1000	760	68

Values are mean or mean ± SD for the IC50 values.

Three independent experiments were performed to determine the IC50 values of Syk.

Table 3. Off-target receptor binding assays.

Receptor	TAS05567 % inh at 10 µM	Receptor	TAS05567 % inh at 10 µM	Receptor	TAS05567 % inh at 10 µM
Adenosine A1	75	Epidermal Growth Factor	-19	Neuropeptide Y Y2	4
Adenosine A2A	2	Estrogen ERalpha	1	Nicotinic Acetylcholine	-10
Adenosine A3	5	Transporter, GABA	15	Nicotinic Acetylcholine Alpha1, Bungarotoxin	0
Adrenergic alpha1A	12	GABAA, Muscimol, Central	-4	Opiate delta1 (OP1, DOP)	0
Adrenergic alpha1B	7	GABAA, Flunitrazepam, Central	24	Opiate kappa (OP2, KOP)	11
Adrenergic alpha1D	10	GABAB1A	-3	Opiate mu (OP3, MOP)	9
Adrenergic alpha2A	-7	Glucocorticoid	9	Phorbol Ester	-9
Adrenergic beta1	-5	Glutamate, Kainate	8	Platelet Activating Factor (PAF)	-10
Adrenergic beta2	15	Glutamate, NMDA, Agonism	3	Potassium Channel [KATP]	-3
Transporter, Norepinephrine	12	Glutamate, NMDA, Glycine	4	Potassium Channel hERG	26
Bradykinin B1	15	Glutamate, NMDA, Phencyclidine	-3	Prostanoid EP4	-2
Bradykinin B2	-3	Histamine H1	-7	Purinergic P2X	5

Calcium Channel L-Type, Benzothiazepine	15	Histamine H2	4	Purinergic P2Y	0
Calcium Channel L-Type, Dihydropyridine	28	Histamine H3	8	Rolipram	34
Calcium Channel N-Type	5	Imidazoline I2, Central	12	Serotonin (5-Hydroxytryptamine) 5-HT1A	-8
Cannabinoid CB1	6	Interleukin IL-1	-10	Serotonin (5-Hydroxytryptamine) 5-HT2B	-9
Dopamine D1	-1	Leukotriene, Cysteinyl CysLT1	11	Serotonin (5-Hydroxytryptamine) 5-HT3	-13
Dopamine D2S	-5	Melatonin MT1	4	Transporter, Serotonin (5-Hydroxytryptamine) (SERT)	-4
Dopamine D3	3	Muscarinic M1	0	Sigma1	-2
Dopamine D4.2	-1	Muscarinic M2	-1	Sodium Channel, Site 2	30
Transporter, Dopamine	24	Muscarinic M3	-7	Androgen (Testosterone) AR	-8
Endothelin ETA	11	Tachykinin NK1	6	Thyroid Hormone	3
Endothelin ETB	0	Neuropeptide Y Y1	-1		

Off-target effects of 10 μM TAS05567 were assessed using the LeadPrifilingScreen commercial assay. Results that show an inhibition or stimulation >50% are considered to represent significant effects on the test compound.

1.3.2 TAS05567 Inhibits BCR-dependent Signaling and FcγR-dependent Functions

As Syk is a key mediator of BCR activation in B cells, we evaluated the effectiveness of TAS05567 in blocking the BCR-dependent signaling cascade. When Ramos cells (human B lymphoma cells) were pretreated with TAS05567 prior to BCR cross-linking by exposure to anti-IgM, there was marked inhibition of the phosphorylation of BLNK, an adaptor protein phosphorylated by activated Syk (Figure 2A). The IC50 of TAS05567 for suppressing induction of BLNK phosphorylation by anti-IgM was 1.8 nM, which was lower than that of R406. We also examined whether TAS05567 inhibited other downstream signaling molecules, including PLCγ2 (IC50, 23 nM) and Erk1/2 (IC50, 9.8 nM), after stimulation of Ramos cells with anti-IgM (Figure 2B, C). TAS05567 showed stronger inhibition of these molecules in the BCR-dependent signaling cascade than R406.

Syk reportedly plays a central role in FcγR-mediated production of proinflammatory cytokines by monocytes and macrophages [62]. Therefore, we evaluated the inhibitory effect of TAS05567 on IgG-induced TNF-α release by THP-1 cells. TAS05567 showed concentration-dependent inhibition of TNF-α production by THP-1 cells stimulated with IgG (Figure 3A). In contrast, TAS05567 had minimal effect on LPS-induced production of TNF-α by these cells, as already reported [63]. These finding suggest that TAS05567

specifically inhibits the FcγR-mediated pathway. Basically, cell-based assays in the present study were carried out under culture conditions with FBS. Hence, we also performed IgG-induced TNF-α production assay using medium containing 10% human serum albumin to give our compound relevance as a potential treatment for inflammatory diseases in humans. The IC50 value of TAS05567 in human settings was 46 nM, which has been almost the same result when using 10% FBS containing medium (Figure 3B). Clearance of antibody-bound platelets in patients with ITP is mediated by phagocytes activated by antibody binding to FcγR [21]. We therefore assessed the effects of TAS05567 on the IgG-FcγR mediated phagocytic acidity in RAW264.7 cells. As shown in Figure 3C, treatment of RAW264.7 cells with TAS05567 resulted in inhibition of FcγR-mediated phagocytosis of IgG-opsonized latex beads.

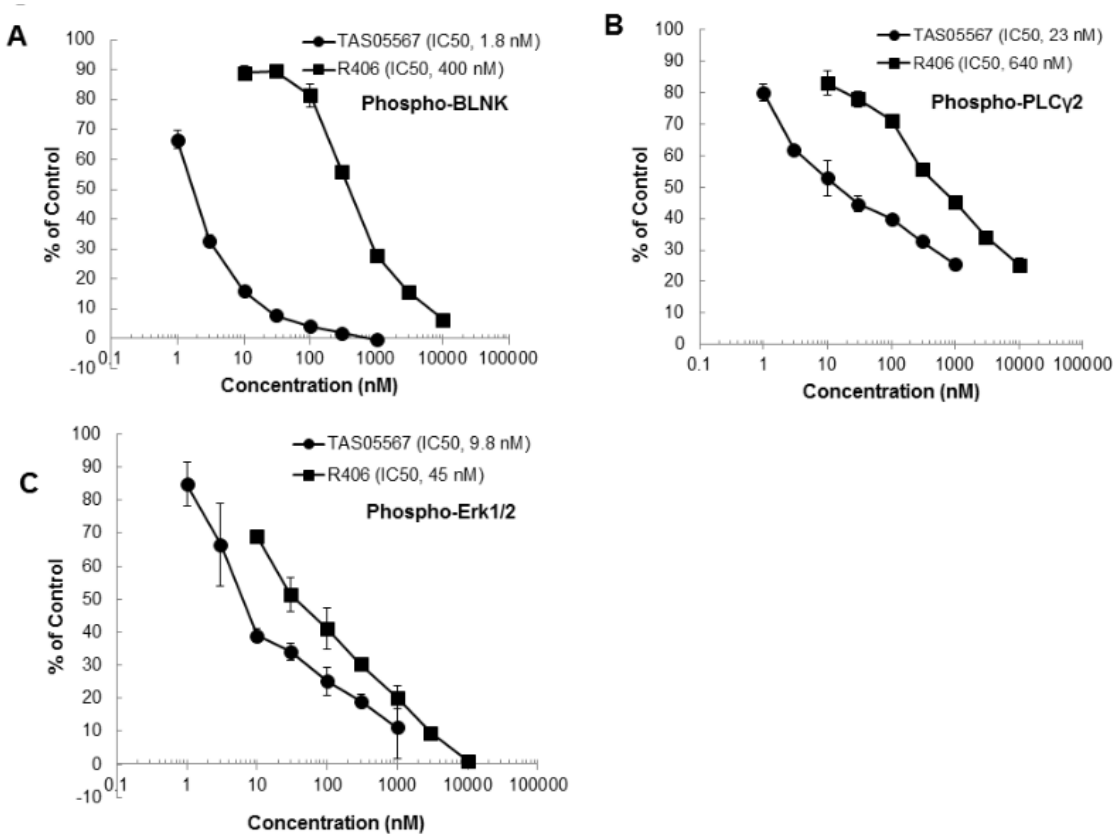

Figure 2. Effects of TAS05567 and R406 on BCR-dependent signaling pathways.

Ramos cells were activated with anti-human IgM F(ab')2 fragments for 10 min in the presence of increasing concentrations of TAS05567 or R406. The phosphorylation levels of BLNK (A), PLCγ2 (B), and Erk1/2 (C) were analyzed by flow cytometry. Values are presented as percent of mean fluorescence intensity relative to vehicle control cells (100%) and non-stimulated control cells (0%). Data are presented as mean ± SD.

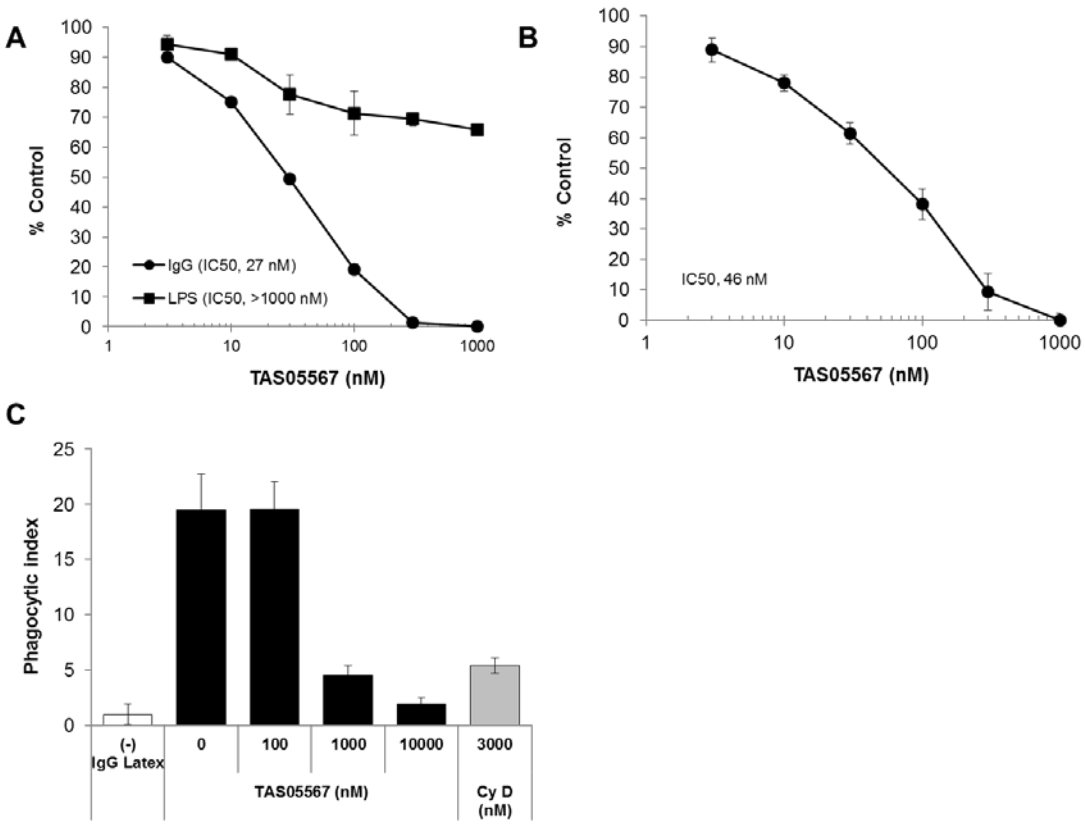

Figure 3. FcγR-mediatd functional activity of TAS05567 in cell-based assays.

(A) THP-1 cells were cultured in RPMI-1640 medium with 10% FBS, and then were seeded in a microwell plate coated with purified human IgG and incubated for 4 h in the presence of increasing concentrations of TAS05567 (circles). THP-1 cells were seeded in an uncoated plate and then stimulated with lipopolysaccharide (LPS) for 24 h in the presence of increasing concentrations of TAS05567 (squares). The level of TNF-α in the culture supernatant was measured by ELISA. (B) THP-1 cells were cultured in RPMI-1640 medium with 10% HSA, and then were seeded in a microwell plate coated

with purified human IgG and incubated for 4 h in the presence of increasing concentrations of TAS05567. The level of TNF-α in the culture supernatant was measured by ELISA. (C) RAW264.7 cells were pretreated with TAS05567 or cytochalasin D (Cy D) for 1 h, followed by incubation with latex beads coated with FITC-labeled IgG (1:500) for 4 h. The cells were collected and analyzed by flow cytometry. Data are presented as mean ± SD.

1.3.3 TAS05567 inhibits IL-1β secretion by NLRP3 inflammasome activation

Recently, Syk has been reported to positively regulate NLRP3 inflammasome activation and promote IL-1β secretion in macrophages and dendritic cells [64], even though NLRP3 inflammasome activation may not be regulated by FcR-dependent signaling pathway. Since aberrant inflammasome activation has been associated with a wide variety of inflammatory diseases [65], we investigated the effect of TAS05567 on IL-1β secretion induced by Alum, one of the NLRP3 ligands, from PMA-treated macrophage-like THP-1 cells. TAS05567 suppressed the IL-1β secretion from the LPS-primed cells in a concentration-dependent manner (Figure 4).

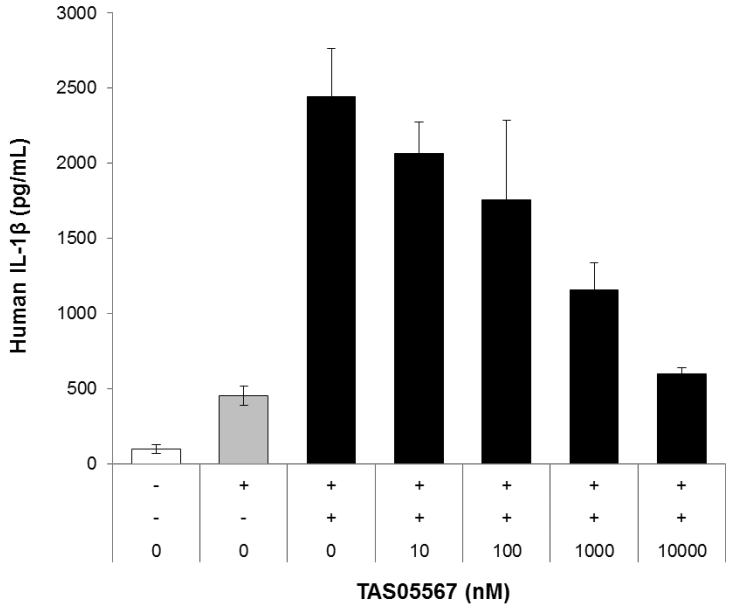

Figure 4. TAS05567 blocks IL-1β production by stimulation with Alum.

THP-1 cells were differentiated with 0.2 μM PMA for 3 days and seeded in a 96-well plate in RPMI-1640 containing 10% FBS overnight. On the next day, the cells were primed with LPS (1 μg/ml) for 3 h and then pretreated with TAS05567 for another 1h. The cells were stimulated with Alum Adjuvant (30 μg/ml) for 9 h. The levels of IL-1β in the culture supernatant were measured by ELISA. Data are presented as mean ± SD.

1.3.4 TAS05567 Suppresses Development of TRAP-positive Multinucleated Cells

In addition to its crucial role in inflammation, Syk contributes directly to bone resorption in RA via its kinase activity–mediated regulation of RANK signaling pathway that is essential for differentiation and activation of osteoclasts [39]. Therefore, we explored the effect of TAS05567 on osteoclast differentiation using human osteoclast precursor cells. After precursor cells were cultured with the indicated concentrations of TAS05567 for 4 days in the presence of M-CSF and RANKL, development of TRAP-positive multinucleated mature osteoclasts was assessed on day 5 (Figure 5A). TAS05567 inhibited the formation of mature osteoclasts in a concentration-dependent manner, and osteoclast differentiation was completely suppressed at 30 nM (Figure 5B).

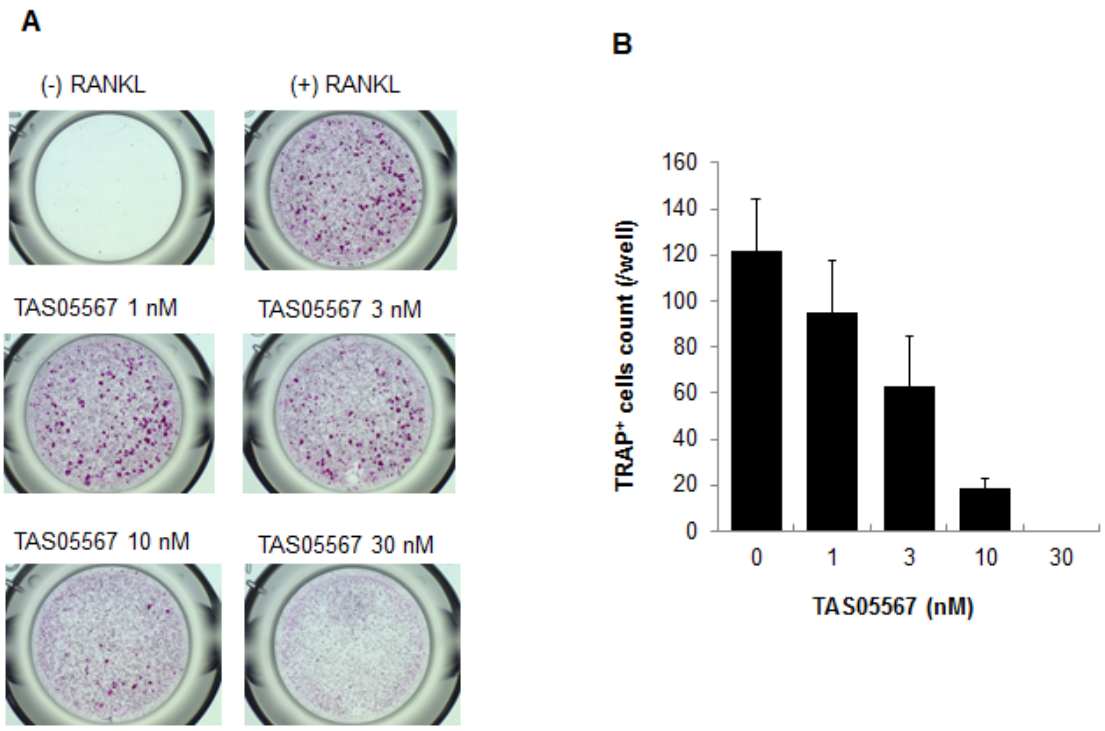

Figure 5. TAS05567 inhibits osteoclastogenesis in a concentration-dependent manner. (A) Representative images of TRAP staining showing M-CSF and RANKL-mediated mature osteoclast differentiation from human osteoclast precursors. Negative control and positive control wells are labeled as (−) RANKL (upper left) and (+) RANKL (upper right), respectively. TAS05567 concentration is labeled on the upper portion of each image. (B) The total number of TRAP-positive osteoclasts per well was determined by manual counting. Data are presented as mean ± SD.

1.2.5 TAS05567 Inhibits IgD-induced BLNK Phosphorylation in Mouse and Rat Whole Blood

As plasma protein binding by drugs has a marked influence on drug activity *in vivo*, we performed whole-blood assays using samples from mice and rats to assess inhibition of BCR-dependent signal transduction as a surrogate pharmacodynamic marker for efficacy in animal models. After peripheral blood samples collected from mice or rats were pretreated with TAS05567 at the indicated concentrations, BLNK phosphorylation was assessed following stimulation with anti-IgD. TAS05567 inhibited anti-IgD–induced BLNK phosphorylation in the peripheral blood B cells of mice and rats in a concentration-dependent manner (Table 4), with estimated IC50 values of approximately 0.2 μM and 0.3 μM, respectively. We also determined the plasma protein binding of TAS05567 using mouse, rat, and human plasma. The mean unbound fraction of TAS05567 in plasma was 15.4% in mouse, 18.3% in rat, and 21.9% in human (Table 5), and therefore the plasma protein binding of TAS05567 was almost the same level between rodents and human.

By integrating the whole-blood assay results with single-dose pharmacokinetic data, we calculated the estimated duration of Syk inhibition by TAS05567 *in vivo.* In mice, the plasma TAS05567 concentration was 0.47 μM at 6 h after administration of 10

mg/kg, indicating that it was above the IC50 in the mouse whole-blood assay for more than 6 h (Figure 6A). When rats were administered TAS05567 at doses of 10 mg/kg or 25 mg/kg, the plasma concentration remained above the IC50 in the rat whole-blood assay for approximately 8 h and 18 h, respectively (Figure 6B).

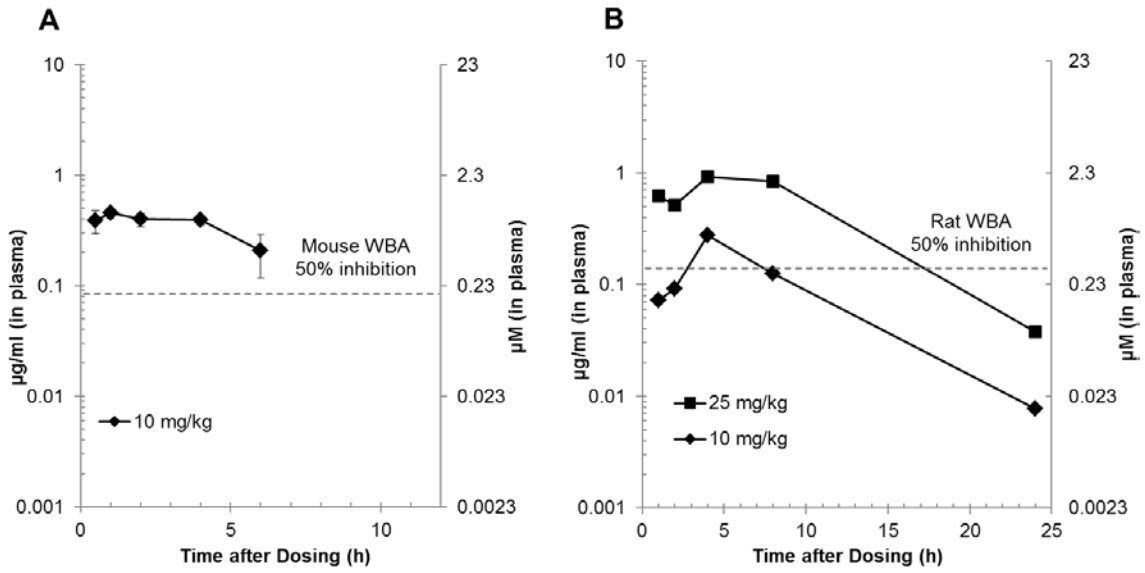

Figure 6. Oral pharmacokinetics of TAS05567 in mice and rats.

(A) Male BALB/c mice were dosed orally with 10 mg/kg of TAS05567, and plasma samples were collected at 0.5, 1, 2, 4, and 6 h after administration. The concentration of the compound in plasma samples was analyzed as described in the Materials and Methods section. Data are expressed as mean ± SEM (n=3). Dashed line shows the IC50 value determined against BCR-mediated BLNK phosphorylation in B cells in mouse whole blood. (B) Male Sprague-Dawley rats were dosed orally with 10 mg/kg or 25 mg/kg, and plasma samples were collected at 1, 2, 4, 8, and 24 h after administration. The concentration of the compound in plasma samples was analyzed as described in the Materials and Methods section. Data are expressed as the mean (n=2). Dashed line shows the IC50 value determined against BCR-mediated BLNK phosphorylation in B

cells in rat whole blood.

Table 4. Effects of TAS05567 on BLNK phosphorylation in mouse or rat whole blood evoked by anti-IgD.

Animal	**Cell Type**	**TAS05567 (μM)**			
		0.1	**0.3**	**1**	**3**
Mouse	CD45R / $B220^{+}$	27%	67%	95%	NA
Rat	$CD45RA^{+}$	NA	49%	82%	104%

Table 5. Plasma protein binding of TAS05567.

Species	Unbound fraction (%)
	TAS05567
Mouse	15.4 ± 0.5
Rat	18.3 ± 1.1
Human	21.9 ± 0.1

TAS05567 was tested at a final concentration of 1 μM in mouse, rat, and human plasma. An aliquot of plasma containing TAS05567 was in the well of equilibrium dialysis device. The plate containing plasma and buffer was equilibrated at 37°C for 6 h, with constant shaking at 80 rpm on an orbital shaker. Samples were collected and precipitated using organic solvents. All samples were centrifuged at 850g for 5 min at 4°C, and then were analyzed by liquid chromatography–tandem mass spectrometry. Data are presented as mean ± SD (n = 3).

1.3.6 TAS05567 suppresses progression in mouse models of CAIA and CIA

To investigate the potential therapeutic value of TAS05567 for RA, we evaluated its effects in representative rodent models of arthritis. CAIA (type II collagen antibody-induced arthritis) is mainly mediated by innate immunity and FcγR-bearing cells are particularly associated with antibody-mediated joint inflammation [65]. When administered orally at doses of 10 and 30 mg/kg/day for 9 days starting from day 0 before injection of a monoclonal antibody cocktail, TAS05567 inhibited the development of arthritis based on clinical scores, with complete inhibition at 30 mg/kg (>90% inhibition; Figure 7A). In addition, serum MMP-3 level was significantly lower in both the10 mg/kg and 30 mg/kg TAS05567 groups than in the vehicle group (Figure 7B).

We also assessed the effect of TAS05567 in a mouse CIA model because this arthritis model has a similar pathogenetic mechanism to human RA due to involvement of several immune cells, including T cells, B cells, and macrophages [66]. TAS05567 was administered prophylactically to the mice at 3 mg/kg or 10 mg/kg/day for 14 days starting from day 0 before the second immunization. When administered at 10 mg/kg, TAS05567 achieved statistically significant improvement of arthritis symptoms compared with the vehicle group (Figure 8A). In addition, the serum level of anti-type

II collagen antibody was significantly reduced at the end of the study in the TAS05567-treated mice (Figure 8B), indicating that suppression of antibody production may have contributed to the improvement of arthritis.

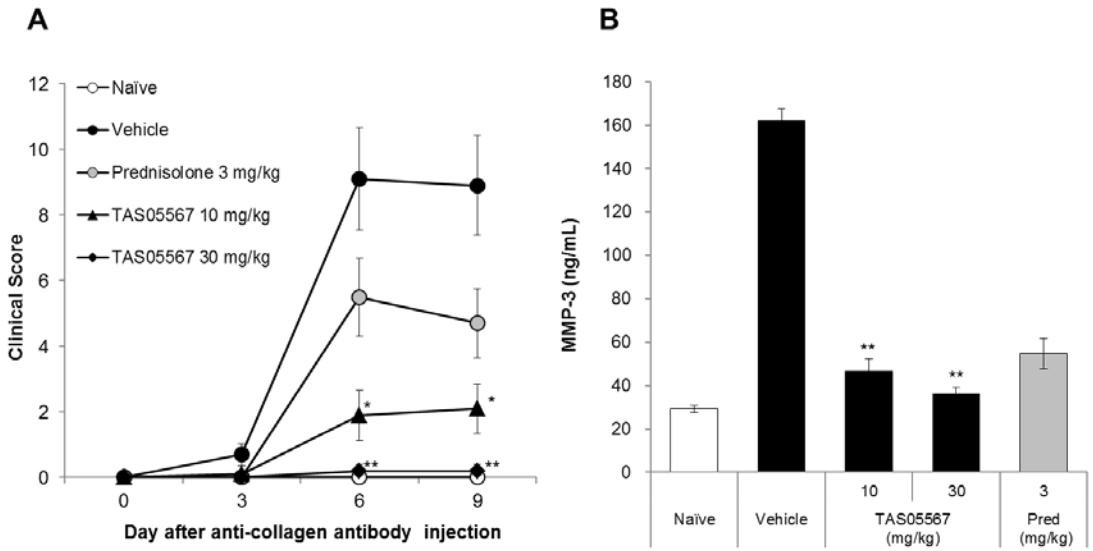

Figure 7. TAS05567 suppresses inflammation in the mouse CAIA model.

(A) Treatment was started from day 0 at the same time as injection of anti-type II collagen antibody and continued for 9 days. Clinical scores were evaluated every 3 days. Groups included naïve, vehicle, prednisolone (3 mg/kg/day), and TAS05567 (10 and 30 mg/kg/day). (B) Serum levels of MMP-3 were determined by ELISA after 9 days of treatment with TAS05567 or vehicle. Data are presented as mean ± SEM (n=10 per group). * P<0.05 and ** P<0.01 compared with the vehicle group.

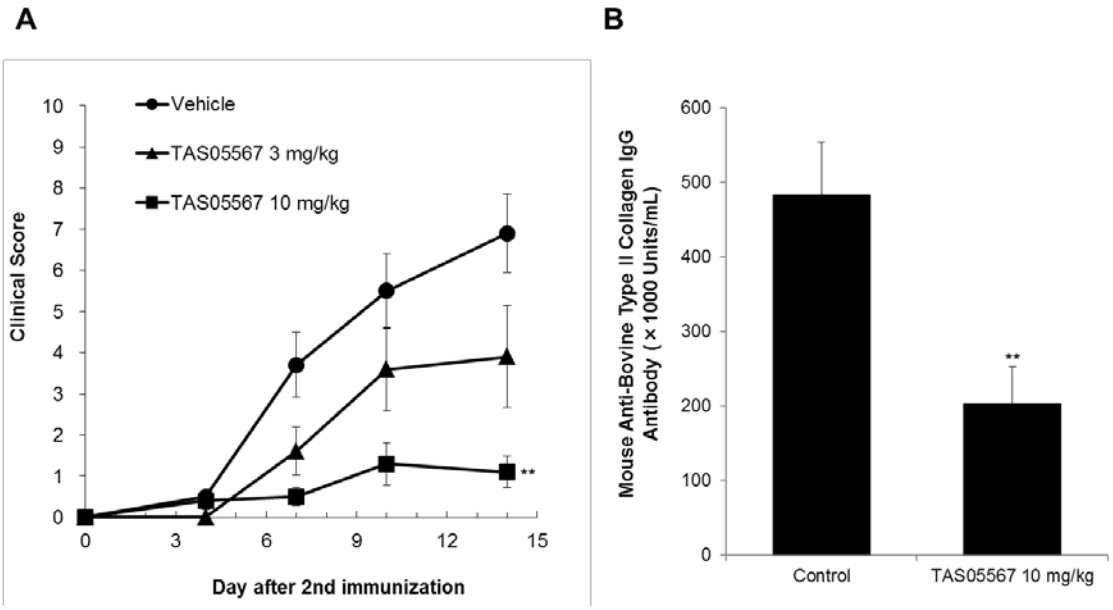

Figure 8. TAS05567 inhibits inflammation and autoantibody production in the mouse CIA model.

(A) Treatment was started from day 0 at the same time as a boost immunization and continued for 14 days. Clinical scores were evaluated twice a week. Groups were given vehicle and TAS05567 (3 and 10 mg/kg/day). Data are presented as mean ± SEM for n = 10 per group. (B) Serum levels of anti-bovine type II collagen IgG after 14 days of treatment with TAS05567 (n = 7) or vehicle (n = 10) were detected by ELISA. Data are presented as mean ± SEM. ** p<0.01 compared with vehicle group.

1.3.7 TAS05567 improves symptoms in a rat model of established CIA

To further explore the therapeutic potential of TAS05567, we tested rats with CIA using a therapeutic dosing regimen. Rats with a significant increase in foot pad volume (indicating paw swelling) were randomly assigned to the vehicle, TAS05567, or R406 groups. Although there was no significant improvement in the 4 mg/kg TAS05567 group, treatment with TAS05567 at doses of 10 mg/kg and 25 mg/kg resulted in significant reduction of joint inflammation (Table 6). In addition, histopathologic examination of the left and right hind paws revealed significant reduction of inflammatory cell infiltration into the synovium and pannus formation in both the 10 mg/kg and 25 mg/kg TAS05567 groups (Figure 9A, B). At these doses, TAS05567 also markedly ameliorated damage to cartilage and bone (Figure 9A, B). R406 treatment also significantly reduced the severity of CIA, markedly abrogating joint swelling as well as cartilage destruction (Table 7 and Figure 11B). Moreover, we evaluated the serum level of COMP, an extracellular matrix glycoprotein associated with disease activity and cartilage damage in RA patients [67]. TAS05567 reduced serum COMP levels in a dose-dependent manner (Figure 9C). R406 also significantly inhibited the production of COMP. Finally, we monitored changes in body weight during treatment as an index of general toxicity and assessed red blood cell count and hemoglobin levels because

anemia was observed in some patients during clinical trials of drugs with JAK2 inhibition [68]. As shown in Figure 10A, the change in body weight was similar between TAS05567- or R406-treated CIA rats and naïve rats. Body weight was higher in TAS05567- or R406-treated rats due to amelioration of systemic inflammation in comparison with vehicle-treated rats. In addition, TAS05567 did not significantly reduce the red blood cell count or hemoglobin level in any dose group compared with the vehicle-treated controls (Figure 10B, C). However, both red blood cell count and hemoglobin level in the R406 group were significantly lower than in the vehicle group.

Table 6. Therapeutic effects of TAS05567 or R406 on antiarthritic activity in collagen-induced arthritis in rat.

Group	Hind paw volume (ml)		
	Day 1	Day 8	Day 14
Naive	2.31 ± 0.03	2.31 ± 0.05	2.28 ± 0.05
Vehicle	2.56 ± 0.07[a]	2.88 ± 0.12	2.92 ± 0.13
TAS05567 (4 mg/kg)	2.55 ± 0.08	2.63 ± 0.08	2.66 ± 0.12
TAS05567 (10 mg/kg)	2.60 ± 0.10	2.41 ± 0.04[b]	2.34 ± 0.03[c]
TAS05567 (25 mg/kg)	2.54 ± 0.07	2.34 ± 0.04[c]	2.33 ± 0.03[c]
R406 (30 mg/kg)	2.58 ± 0.09	2.41 ± 0.08 [c]	2.49 ± 0.10 [b]
Prednisolone (3 mg/kg)	2.54 ± 0.06	2.44 ± 0.03[c]	2.47 ± 0.05[c]

Data are presented as mean ± SEM. n=6 rats in the naïve group; n=9 rats each in the vehicle and treatment groups. a $P<0.01$ compared with the naïve group. b $P<0.05$ compared with the vehicle group. c $P<0.01$ compared with the vehicle group.

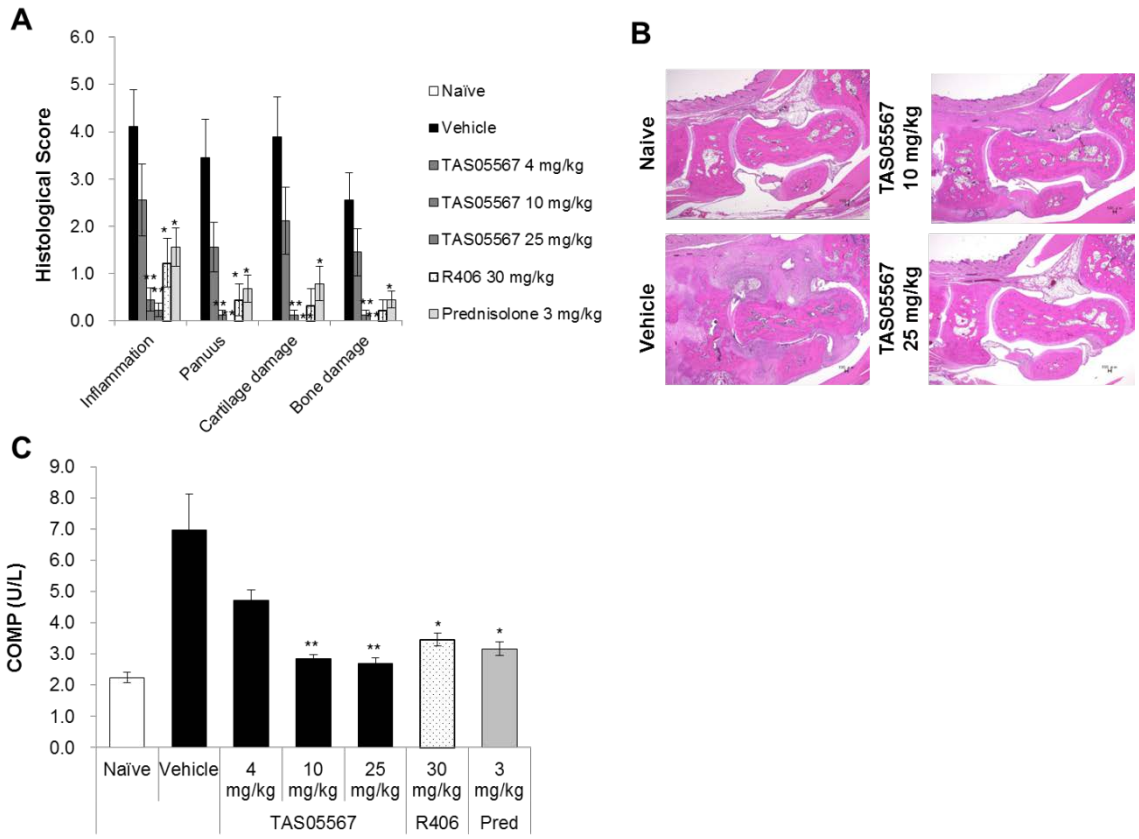

Figure 9. TAS05567 improves disease severity in a dose-dependent manner in the established rat CIA model.

(A) Both hind paws from each rat after 14 days of treatment with vehicle, TAS05567, R406, or prednisolone were processed for histologic evaluation of joint inflammation, pannus formation, cartilage damage, and bone damage. Histologic changes for each parameter were scored (range, 0-8). (B) Representative photomicrographs of hematoxylin-eosin staining are shown (original magnification ×40). (C) Serum levels of COMP after 14 days of treatment in naïve, vehicle, prednisolone, R406, and TAS05567

groups as determined by ELISA. Data are presented as mean ± SEM. n=6 rats in the naïve group; n=9 rats each in the vehicle and treatment groups. * $P<0.05$ and ** $P<0.01$ compared with the vehicle group.

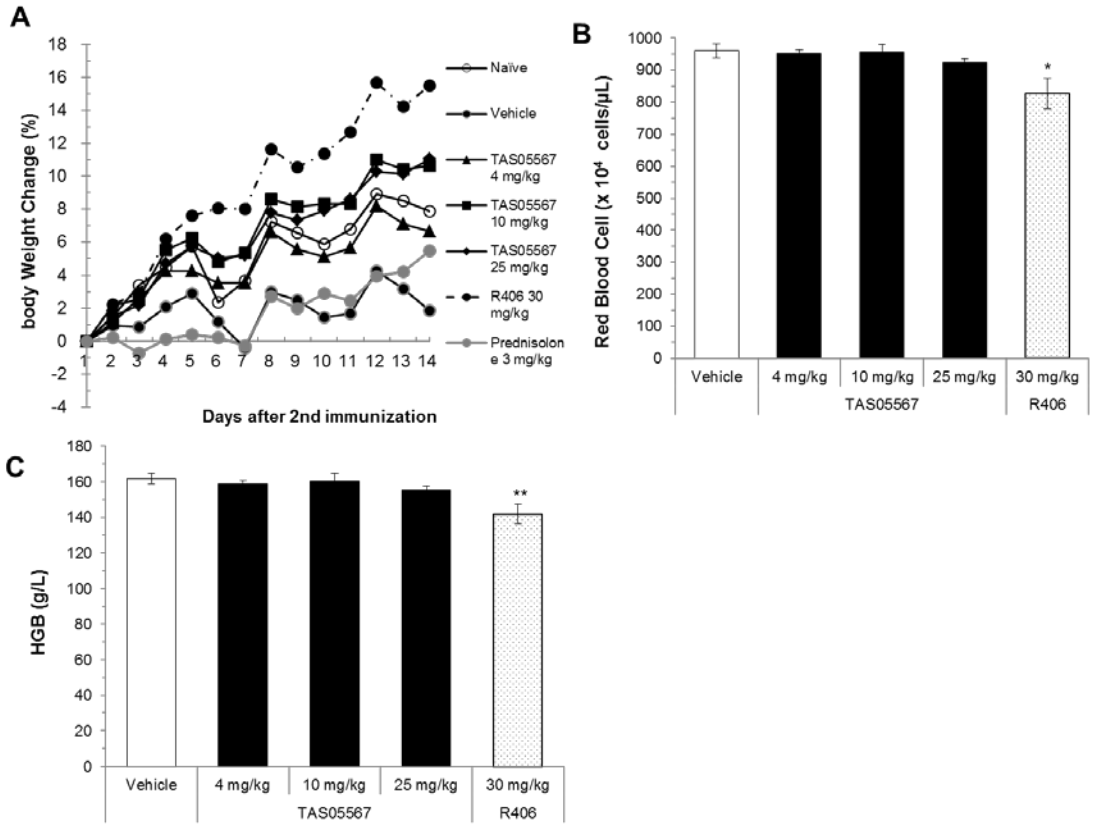

Figure 10. TAS05667 does not affect body weight, red blood cell count, or hemoglobin level in the established rat CIA model. (A) CIA rats with clinical sings of paw swelling were randomized at day 1. Treatment was started from day 1 and continued for 14 days. Changes in body weight of the rats were monitored every day. Body weight changes (0% at day 1) for each group are presented as average values. Peripheral blood samples from were obtained from the rats and analyzed for changes in red blood cell count (B) and hemoglobin level (C). Data are presented as mean ± SEM. n=6 rats in the naïve group; n=9 rats each in the vehicle and treatment groups. * P<0.05 and ** P<0.01

compared with the vehicle group.

1.3.8 TAS05567 Ameliorates Thrombocytopenia in a Mouse Model of ITP

ITP is an autoantibody-mediated disorder in which IgG binds to platelets and causes their accelerated clearance via FcγR expressed on macrophages [21]. TAS05567 inhibited FcγR-dependent phagocytosis in macrophages (Figure 3C). Accordingly, we examined whether TAS05567 could attenuate platelet count decreases in mice with thrombocytopenia induced by administration of an antiplatelet antibody. In mice injected with an anti-CD41 antibody, the platelet count decreased by more than 50% compared with sham mice, whereas the platelet count in IVIg-treated mice was significantly higher than that of vehicle-treated mice (Figure 11). In this model, TAS05567 provided significant protection against anti-CD41 antibody–induced thrombocytopenia in a dose-dependent manner and completely prevented thrombocytopenia when administered at 100 mg/kg (Figure 11). Some signs of toxicity, such as body weight loss and lower locomotor activity, were not observed during the treatment period (data not shown). The platelet count in R406-treated mice was also significantly higher than that of vehicle-treated mice, but this drug only partially prevented thrombocytopenia even at 100 mg/kg (Figure 11).

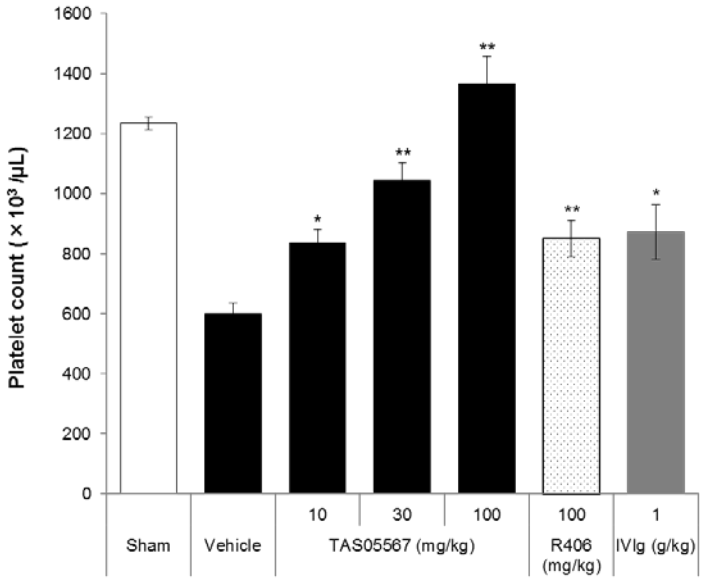

Figure 11. TAS05567 protects mice from anti-platelet antibody–induced thrombocytopenia.

Mice were treated with TAS05567 (10, 30, 100 mg/kg) or R406 (100 mg/kg) on days 1 and 2. For the IVIg group, mice were intravenously injected with 1 g/kg IVIg once on day 1 only. On day 2, mice were intravenously injected with anti-CD41 antibody. Platelet counts were evaluated 24 h later. Data are presented as mean ± SEM (n=5 or 6 per group). * $P<0.05$ and ** $P<0.01$ compared with the vehicle group.

1.3 Discussion

In this chapter, we determined the pharmacological profile of a novel selective Syk inhibitor, TAS05567, which potently inhibited BCR signaling as well as FcγR-dependent cellular functions. TAS05567 also inhibited osteoclast differentiation and blocked IL-1β release triggered by NLRP3 inflammasome activation. After oral administration, TAS05567 was well tolerated and ameliorated symptoms in animal models of RA and ITP, which are both humoral immune-mediated autoimmune diseases.

Our biochemical assays revealed that R406 showed inhibitory activity against several protein kinases, including VEGFR2 and JAK2, which are associated with the potential risk of hypertension and anemia [46, 47]. Among several inhibitors of the kinase activity of Syk under development, Fostamatinib has demonstrated effectiveness for ITP in Phase III trials [55], but hypertension was more frequent in the Fostamatinib group than in the placebo group during clinical trials for RA [56]. In addition, anemia was observed in the patients treated with Tofacitinib and Baricitinib owing to inhibition of JAK2 kinase activity [69, 70]. Compared with R406, TAS05567 not only showed lower activity against theses kinases, but also displayed more potent inhibition of Syk activity (Figure 1, Table 1, and Table 2). Regarding Syk and the selected 4 kinases, including

VGFR2 and JAK2, we also performed the enzymatic assays at 1 mM ATP to approximate cellular concentrations. In this condition, TAS05567 inhibited Syk activity with IC50 of 1.5 nM, but much less activity against the 4 kinases, demonstrating that TAS05567 has highly selective inhibitory activity against Syk kinase at the cellular level. Indeed, in the rat model of established CIA, body weight and hematology parameters for anemia were not affected by 2 weeks of treatment with TAS05567 (Figure 10A, B, and C), suggesting that it is well tolerated. In addition to assessing selectivity for protein kinases, we performed cellular assays to obtain data about targeting of the immune system by TAS05567. Interestingly, although TAS05567 markedly reduced FcγR-mediated proinflammatory cytokine, TAS05567 had little effect on the response to TLR4 stimulation (Figure 3A). Innate immune responses mediated through TLR4, which is mainly expressed on monocytes and neutrophils, are associated with host defenses against microbial infection, particularly gram-negative bacteria [71]. Therefore, this feature of TAS05567 could be an advantage for treating patients with autoimmune diseases such as RA because an increased risk of infection has been one of the major issues with conventional therapies [6, 8]. To delineate the toxicity profile of TAS05567 in detail, further toxicity studies in rodents or non-rodent species will be required.

In the joints of patients with RA, autoantibodies form ICs that interact with FcRs expressed on synovial immune cells to induce production of proinflammatory cytokines, resulting in disease progression [72]. Similar to human RA, anti-type II collagen antibodies form ICs that activate FcγRs on macrophages and monocytes in animal models, causing synovitis in CAIA and CIA [65, 73]. Consistent with the inhibitory effect of TAS05567 on FcγR-mediated immune responses *in vitro*, treatment with this drug dose-dependently suppressed paw swelling in both rodent models (Figure 7A, 8A, and Table 6). Of note, in pharmacokinetic studies and whole-blood assays, the robust effect of TAS05567 in these arthritis models was achieved without continuous inhibition of the target (Figure 6), which is consistent with a previous report [74]. Therefore, TAS05567 may provide significant benefit for patients with RA at doses that partially suppress Syk activity, thus mitigating the toxic effects associated with complete genetic deletion of Syk. In the present study, it is interesting that TAS05567-treated CIA mice also showed significant reduction of anti-type II collagen IgG production (Figure 8B). Syk has been reported to be involved in antibody production via TLR9 signaling and is required for differentiation of plasma cells in the presence of antigens [75]. Accordingly, our data suggest that direct inhibition of autoantibody production by a Syk inhibitor may contribute to improvement of arthritis symptoms, in addition to blockade of

FcR-mediated signaling in effector cells.

This study demonstrated that TAS05567 strongly suppresses damage to bone in a rat model of established CIA (Figure 9A, B). Syk is recruited and phosphorylated as a result of the RANKL-RANK interaction, after which it induces activation of c-Fos and nuclear factor of activated T cells cytoplasmic 1, leading to differentiation of functional osteoclasts [76]. Consistent with the findings obtained in Syk-deficient cells [34], in the present study, TAS05567 blocked the differentiation of mature osteoclasts from immature cells in the presence of RANKL (Figure 5). In a recent clinical trial, an anti-RANKL antibody (Denosumab) achieved clinically meaningful and significant reduction of bone erosion in RA patients, suggesting that drugs which target the RANKL pathway could become novel options for RA patients with risk factors for joint destruction [77]. However, Denosumab failed to improve joint space narrowing, which reflects cartilage damage [77]. In the present study, there was histological improvement of the ankle joints in TAS05567-treated CIA rats and the serum COMP concentration decreased to almost the same levels as in naive rats (Figure 9C). Several studies have shown that elevation of the serum COMP level reflects joint damage, particularly cartilage degradation [67, 78]. Furthermore, TAS05567 reduced the serum MMP-3 level in CAIA mice in the present study (Figure 7B). MMP-3 plays a pivotal role in the

degradation of cartilage components, and this enzyme is produced when synovial cells are stimulated by proinflammatory cytokines such as TNF-α and interleukin-1β [79]. Indeed, it was reported that R406 blocks TNF-α–induced MMP-3 production in fibroblast-like synoviocytes from RA patients by suppressing Syk pathway activation [80]. Thus, improvement of cartilage damage in our rat CIA model may have been associated with suppression of MMP-3 production by TAS05567, although the serum MMP-3 level was not determined in this study. Taken together, these findings suggest that TAS05567 would be useful for alleviating both progressive bone erosion and cartilage damage in RA.

In addition to its potential usefulness for treating RA, TAS05567 inhibited FcγR-dependent phagocytosis in macrophages (Figure 3C) and exhibited significant efficacy in a representative animal model of ITP at the same dosage used in the mouse arthritis model (Figure 11). Lu and colleagues reported that decreasing Syk expression in macrophages by transfection with Syk-specific siRNA attenuates antibody-mediated phagocytosis, a finding that is consistent with our data [81]. Of note, treatment with TAS05567 at 100 mg/kg completely prevented the induction of thrombocytopenia by injection of anti-CD41 antibody in the present study. Fostamatinib also showed efficacy in a similar model of ITP, but it only partially prevented thrombocytopenia even at 100

mg/kg in this study (Figure 11). Fostamatinib was reported to be effective against refractory ITP in clinical trials, but not all patients responded to it [45]. Considering the balance between efficacy and safety, 100 mg/kg may be too high a dose of TAS05567, even though no toxicity was observed during the treatment period in our experiments. However, TAS05567 has much higher selectivity for the target enzyme than Fostamatinib, suggesting that it would be better tolerated and can be used at higher doses without causing off-target side effects. Taken together, these results suggest that TAS05567 could become a novel option for the treatment of a broad range of ITP patients, including those refractory to conventional therapies.

We also demonstrated that TAS05567 inhibited secretion of IL-1β by macrophage-like cells stimulated with alum (Figure 4). Recent research has shown that Syk mediates NLPR3 stimulus-induced activation of caspase-1 in ICs-independent manner and consequently inhibits secretion of IL-1β and IL-18 via the association with NLRP3 and adaptor protein ASC [64]. The NLRP3 inflammasome has been reported to be involved in the pathogenesis of several inflammatory diseases, including RA, inflammatory bowel disease, gout, cryopyrin-associated periodic syndromes (CAPS), and Alzheimer's disease [82]. Indeed, IL-1 blockers have been approved by the U.S. Food and Drug Administration to treat RA and CAPS [83]. Consequently, besides being

a possible new therapeutic option for specific autoimmune diseases, TAS05567 may be an attractive candidate for a wide range of inflammatory disorders related to the NLRP3 inflammasome. Therefore, we need to investigate the detailed molecular mechanisms by which TAS05567 modulates NLRP3 inflammasome responses using cellular assays to examine whether this drug could be an option for treating diseases caused by inflammasome overactivation.

Our data support the possibility that TAS05567 could become a novel treatment for diseases such as RA, ITP, and other inflammatory disorders related to abnormal activation of Syk.

Chapter 2

Therapeutic effects of TAS05567 on allergic diseases as well as B-cell malignancies using preclinical animal models

2.1 Introduction

Type 1 allergic diseases, such as allergic rhinitis, atopic dermatitis, asthma, and allergic anaphylaxis, are called the epidemics of the 21st century [29, 84]. Allergic symptoms range from local reactions of the mucosa to generalized symptoms in the skin, airways, gastrointestinal tract, and circulation system, and it is estimated that up to 25% of the population may be affected by them. [85, 86]. The role of antigen-specific IgE in type 1 allergic diseases has been revealed, with antigen-mediated IgE cross-linking inducing the degranulation of mast cells/basophils [28]. The IgE-primed these cells release granules and several chemical mediators, including histamine, leukotrienes, and cytokines, which cause the characteristic allergic reactions, such as hives, wheezing, abdominal symptoms, and even anaphylaxis diseases [30]. Of note, FcεRI or Syk deletion in mice reduces allergic responses in animal models of allergy [31, 40]. From these findings, Syk is implicated as a key regulator of the disease progression in patients with type 1 allergic diseases, and therefore, inhibitors targeting Syk kinase may be

promising and attractive therapeutic option for the treatment of these diseases.

BCR signaling cascades are activated and required for cell survival in some B-cell lymphoma, such as DLBCL [41]. DLBCL is the most common subtype of non-Hodgkin lymphoma (NHL), and the estimated incidence is ~7 per 1000,000 person-years in Western countries [87, 88, 89]. The standard of care for initial treatment of DLBCL is rituximab, cyclophosphamide, doxorubicin, vincristine, and prednisone, which achieves a cure in many patients [90]. However, despite potentially curable, ~40% of patients with DLBCL were died of relapse or refractory disease [43, 91]. Syk protein is activated in an approximately half of primary human DLBCL tissues by a tissue microarray analysis, suggesting that Syk kinase holds promise as a therapeutic target for DLBCL [42]. Indeed, Syk inhibitors, such as GS-9973, have also been developed for the therapy of the lymphoma including DLBCL [48, 92].

In this chapter, we examined the therapeutic potential of TAS05567 against type 1 allergic diseases and DLBCL tumors using *in vitro* assays as well as preclinical animal models. In *in vitro* experiments, we investigated whether not only TAS05567 could block antigen-induced calcium flux and histamine release in IgE-sensitized basophilic cells, but also inhibit cell cycle progression as well as proliferation of DLBCL cells through Syk-mediated signaling cascades. Moreover, we investigated whether

TAS05567 could suppress the ear swelling provoked by antigen as an index of type 1 allergic reaction in TNP-specific IgE transgenic mice. Finally, the *in vivo* antitumor activity of TAS05567 was evaluated in SCID mice bearing SU-DHL-10, one of the DLBCL cell lines, xenograft.

2.2 Materials and Methods

2.2.1 FcεRI-mediated Calcium Flux and Histamine-release Assay

The intracellular calcium level was determined using a FLIPR® Calcium 6 Assay kit (Molecular Devices, Sunnyvale, CA, USA). RBL-2H3 cells (ATCC CRL-2256) were seeded overnight at 5×10^4 cells/well in a 96-well clear-bottomed plate with black walls in Minimum Essential Media containing 15% FBS. After washing with serum-free MEM, the cells were sensitized by incubation for 1 h at 37°C with mouse anti-2,4-dinitrophenyl (DNP) -IgE (0.3 μg/ml, Sigma-Aldrich), followed by incubation with FLIPR® Calcium 6 Assay kit dye and TAS05567 for 2 h at 37°C. DNP–bovine serum albumin (BSA) (0.1 μg/ml, LSL, Tokyo, Japan) was added and fluorescence (relative fluorescence units: RFUs) was detected every 30 s at an excitation wavelength of 485 nm and an emission wavelength of 525 nm using a Flex Station II (Molecular Devices). ΔRFU was calculated by subtracting the value at initiation of measurement.

For the histamine-release assay, RBL-2H3 cells were seeded overnight in a 96-well plate (2×10^4 cells/well). After washing, the cells were sensitized by incubation with mouse anti-DNP-IgE (0.3 μg/ml) for 1 h at 37°C. The sensitized cells were then pretreated with TAS05567 for 1 h, followed by stimulation with DNP-BSA (0.1 μg/ml) for 15 min at 37°C and measurement of histamine in the supernatant using a histamine

EIA kit (Medical & Biological Laboratories, Nagoya, Japan).

2.2.2 Detection of Syk and BLNK Phosphorylation (SU-DHL-10 cells)

SU-DLH-10 (ATCC CRL-2963) was purchased from the American Type Culture Collection and maintained in RPMI-1640 medium (Sigma-Aldrich) containing 10% FBS. SU-DHL-10 cells (8×10^4 cells/100 µl) were pretreated with test compounds, followed by stimulation with goat $F(ab')_2$ anti-human IgG (5 µg/ml; Southern Biotech) for 10 min at 37°C. For the detection of Syk phosphorylation, the cells were lysed in lysis buffer (EMD Millipore, Burlington, Germany) supplemented with a mixture of protease inhibitors. The level of Syk phosphorylation (Y525/Y526) in the cell lysate was determined by enzyme-linked immunosorbent assay (ELISA) (Cell Signaling Technology, Danvers, MA, USA). For the detection of BLNK phosphorylation, the cells were fixed after the stimulation with anti-human IgG. Then, the cells were washed in staining buffer (FBS) (BD Biosciences) and incubated for 1 h at RT in the same buffer containing Alexa Fluor 488–labeled mouse anti-BLNK (pY84) (clone J117-1278) (BD Biosciences). Subsequently, the cells were resuspended in staining buffer (FBS). Phosphorylation of BLNK induced by anti-IgM antibody was quantified using a Guava® easyCyte flow cytometry systems (EMD Millipore).

2.2.3 Cell Viability Assay

SU-DHL-5 (ATCC CRL-2958), SU-DHL-6 (ATCC CRL-2959), SU-DHL-10 (ATCC CRL-2963), and Pfeiffer (ATCC CRL-2632) were purchased from the American Type Culture Collection. Each cell line was seeded in 96-well plates at a density of between 3 × 10^3 and 8 × 10^3, cultured in RPMI 1640 containing 10% FBS for 24 h at 37ºC, and then incubated with TAS05567 for another 72 h in the same medium. Cell viability was analyzed with CellTiter-Glo® luminescent cell viability assay kit (Promega KK, Tokyo, Japan). After cultivation for 72 h, an equal volume of CellTiter-Glo® reagent was added, the plates were shaken and luminescence was measured using a microplate luminometer.

2.2.4 Cell Cycle Analysis

SU-DHL-10 cells were exposed to TAS05567 for 24 h or 72h. The cells were collected, washed with PBS and stained for cell cycle analysis using Cycletest™ Plus DNA Reagent Kit (BD Biosciences). The stained cells were analyzed by a flow cytometer (BD Biosciences). The proportion of cells in SubG1, G1, S, and G2/M phases was represented as DNA histograms.

2.2.5 Quantitative real-time PCR

Relative gene expression was performed to use 7900HT Fast Real-time PCR System (Applied Biosystems, Foster City, CA, USA) [93]. TaqMan® gene expression assays for

EGR2 (Assay ID; Hs00166165_m1) was used, respectively. In brief, total RNA samples were obtained from SU-DHL-10 cells, which were treated with TAS05567 for 8 h, and then cDNA samples were synthesized. PCR reaction mixture was prepared with 2×TaqMan® Fast Universal PCR Master Mix, 1 μL of the synthesized cDNA as the template, and each primer at a final concentration of 0.9 μmol/L. The conditions for real-time PCR were 1 cycle at 50ºC for 2 min and 95ºC for 10 min; and 40 cycles at 95 ºC for 15 s and 60 ºC for 10 min. Gene expression profiling was performed using the comparative CT method for relative quantification. The calibration samples were untreated cells, and 18S ribosomal RNA was used as an endogenous control.

2.2.6 Experimental Animals

All animal experiments were approved by the Animal Experiments Ethics Committee of Taiho Pharmaceutical Co., Ltd. The animals used for the present study were male C.B-17 SCID mice from Charles River Laboratories Japan (Yokohama, Japan) and male TNP-specific IgE transgenic mice from CLEA Japan (Tokyo, Japan). All animals were housed in cages and maintained under a 12-h light/dark cycle with water and food supplied ad libitum. During the experimental period, animals were observed to assess activity, feeding, and signs of pain in accordance with the established protocol. For administration, TAS05567 was dissolved in a solution of 0.5% hydroxypropyl methyl

cellulose (Shinetsu Chemical, Tokyo, Japan) with 0.1 N HCl, and prednisolone was suspended in a solution of 0.5% HPMC without HCl.

2.2.7 Mouse Model of Type I Allergy

Male TNP-specific IgE transgenic mice (7 weeks old) were epicutaneously administered 0.025% picryl chloride (1-chloro-2,4,6-trinitrobenzene; Nakalai Tesuque, Kyoto, Japan) in acetone on both ears (10 μl per ear). TAS05567 was administered orally to mice 30 min before antigen challenge. Ear thickness was measured using a dial thickness gauge G-2 (Ozaki, Tokyo, Japan) at 1, 2, 4, and 24 h after antigen challenge. Difference in ear thickness (average value on the right and left) was calculated at each time point.

2.2.8 Mouse Subcutaneous Xenograft Model

SU-DHL-10 cells (2×10^7 cell) were prepared into single cell suspension in 0.1 ml of PBS:matrigel (Corning Incorporated, Corning, NY, USA) and injected subcutaneously on the flank of the mice. Mice that had tumors with an estimated volume of approximately 200 mm^3 [the largest tumor diameter in mm × (the smallest diameter in $mm)^2$ / 2] were selected and assigned to groups of five animals each by stratified random allocation based on individual tumor volumes so that each group had an almost equal mean tumor volume on day 1 of dosing. Tumor volumes were measured twice

weekly in vehicle-treated and TAS05567-treated groups. At the end of the experiment, tumor xenografts were excised, and then tumor weight was measured. Body weight was measured twice a week to monitor toxicity.

2.2.9 BLNK Phosphorylation and EGR2 Gene Expression in Tumors

For detection of BLNK phosphorylation events in the SU-DHL-10 tumors, mice were sacrificed at 6 h after the first administration or 18 h after the second administration (24 h post-first administration), followed by tumor resection. The tumor tissues (approximately 100 mg) were excised and dispersed by gentleMACS Dissociator (Miltenyi Biotec GmbH, Germany). The cells isolated from the tumor tissues were treated with goat $F(ab')_2$ Anti-Human IgG (10 μg/ml; Southern Biotech) for 10 min at 37°C. The cells were fixed, and then incubated for 1 h at RT in the same buffer containing Alexa Fluor 488–labeled mouse anti-BLNK (pY84) (clone J117-1278) (BD Biosciences). Phosphorylation of BLNK induced by anti-IgG antibody was quantified using a flow cytometry using a Guava® easyCyte flow cytometry systems (EMD Millipore). For analysis of the gene expression of ERG2, mice were sacrificed at 14 h after the second administration (20 h post-first administration), followed by tumor resection. mRNA was extracted from the tumor tissues, and then cDNA samples were synthesized. Relative gene expression was performed using 7900HT Fast Real-time

PCR System (Applied Biosystems). TaqMan® gene expression assays for EGR2 (Assay ID; Hs00166165_m1) was used. The calibration samples were untreated cells, and 18S ribosomal RNA was used as an endogenous control.

2.2.10 Statistical Analysis

Statistical analysis and determination of half-maximal IC50 values were performed with EXSUS software, version 8.0.0 (CAC Exicare, Tokyo, Japan). Results are reported as mean ± SD for *in vitro* experiments or mean ± SEM for *in vivo* experiments.

The efficacy of TAS05567 in *in vivo* studies was evaluated using Dunnett's test. In all analyses, $P<0.05$ was considered to indicate statistical significance.

2.3 Results

2.3.1 TAS05567 Inhibits IgE-Dependent Cellular Functions

Syk-deficient mast cells from inducible Syk knockout mice generated using the Cre/loxp system showed no calcium flux or histamine release despite activation of FcεRI [94]. Therefore, we evaluated the ability of TAS05567 to block FcεR-mediated cellular functions by examining its effect on antigen-induced calcium flux and histamine release in IgE-sensitized RBL-2H3 cells (rat basophilic cells). As shown in Figure 12A and 12B, TAS05567 suppressed both calcium flux (IC50, 27 nM) and histamine release (IC50, 13 nM) induced by cross-linking of FcεRI with IgE and antigen.

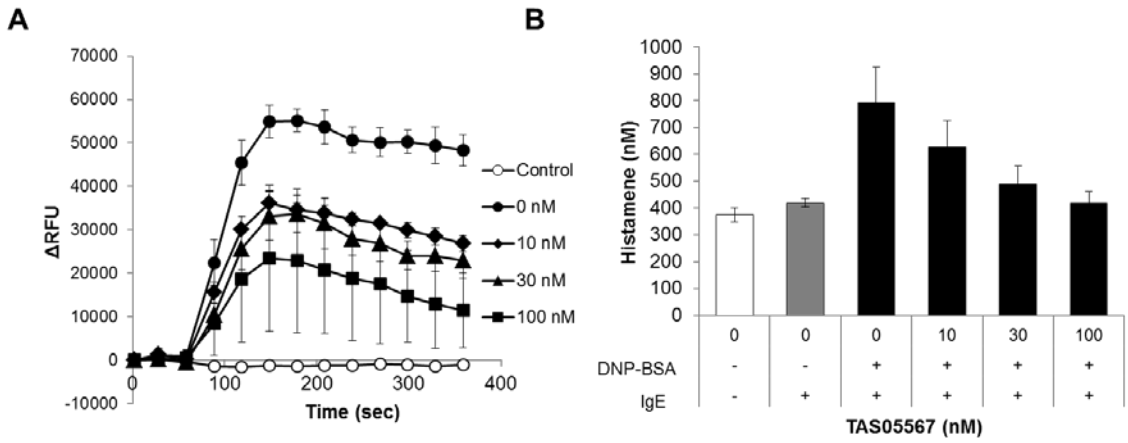

Figure 12. IgE-mediated functional activity of TAS05567 in basophilic cells.

(A) RBL-2H3 cells were treated with anti-DNP IgE for 1 h. Calcium 6 kit dye and TAS05567 were added and incubated for 2 h, followed by stimulation of cells with DNP-BSA. Monitoring of RFUs was as described in the Materials and Methods section.

(B) RBL-2H3 cells were treated with anti-DNP IgE for 1 h. The sensitized cells were then pretreated with TAS05567 for 1 h, then stimulated with DNP-BSA for 15 min. Histamine content in the supernatant was measured using a histamine EIA kit. Data are presented as mean ± SD.

2.3.2 TAS05567 Attenuates IgE Cross-linking–induced Skin Lesions in TNP-IgE Transgenic Mice

In the cell-based assay, TAS05567 inhibited histamine release from IgE-sensitized RBL2H3 cells stimulated with antigen (Figure 12B). We therefore evaluated the effects of TAS05567 on IgE-dependent allergic reactions *in vivo* using TNP-IgE transgenic mice. Administration of picryl chloride to the ears of TNP-IgE transgenic mice provoked ear swelling, which reached a peak 2 h after antigen challenge (immediate phase), and swelling was observed even after 24 h (late phase) (Figure 13). TNP-IgE transgenic mice were treated orally with a single dose of TAS05567 (10 mg/kg or 25 mg/kg) 30 min before antigen challenge. As shown in Figure 13, TAS05567 strongly suppressed ear swelling from 1 to 4 h after challenge but did not show any significant effect on swelling at 24 h.

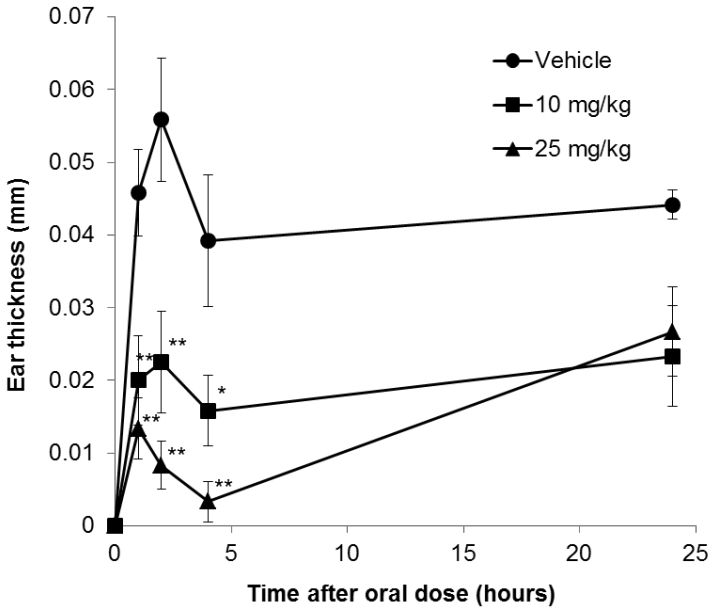

Figure 13. TAS05567 blocks the increase in ear thickness in TNP-IgE transgenic mice. TNP-specific IgE transgenic mice were treated with TAS05567 (10, 25 mg/kg) 30 min before epicutaneous administration of 0.025% picryl chloride. Ear thickness was measured at 1, 2, 4, and 24 h after antigen challenge. Difference in ear thickness (average value on the right and left) was calculated at each time point. Data are presented as mean ± SEM (n=6 per group) * $P<0.05$ and ** $P<0.01$ compared with the vehicle group.

2.3.3 TAS05567 Inhibits Cell Cycle Progression and Proliferation of DLBCL cells Through Syk-mediated Signaling Pathway

Syk is expressed in multiple DLBCL cell lines and activated in primary DLBCL tissues. Additionally, the proliferation of Syk siRNA-transfected cells is suppressed in some DLBCL cells [42]. Based on these evidences, we evaluated the inhibitory effects of TAS05567 on 5 DLBCL cell lines at a wide range of concentrations (Figure 14). We repeated the same experiment twice and obtained almost the same results. Among these cell lines, Pfeiffer and SU-DHL-10 had IC50 values below 100 nM (Table 7); SU-DHL-5, SU-DHL-6, and, DOHH2 had IC50 values between 100 nM and 300 nM in both experiments.

Following these results, we next analyzed cell cycle progression of DLBCL cells in the presence of TAS05567. We focused on SU-DHL-10 cells for subsequent experiments, because this cell line responded well to TAS05567 in the cell proliferation assay as shown in Figure 14 and enabled *in vivo* experiments due to developing tumor nodules after subcutaneous injection of SU-DHL-10 cells to mice (data not shown). As shown in Figure 15A and 15B, the fraction of cells in the S phase was reduced by 24 h and 72 h treatment of cells with increasing doses of TAS05567. Percentages of cells in sub-G1 phase and G1 phase were increased in a concentration-dependent manner by

treatment with TAS05567. These results suggest that TAS05567 caused cell-cycle arrest at the sub-G1/G1 phase in SU-DHL-10 cells.

We further determined whether TAS05567 inhibited the Syk downstream pathway in SU-DHL-10 cells. Tyrosine 525/526 on Syk is an auto-phosphorylation site and phosphorylation of its residues is observed in several DLBCL cell lines as well as primary DLBCL tissues [42]. Therefore, we measured the levels of phosphorylation at Y525/526 on Syk induced by IgG in SU-DHL-10 cells. As shown in Figure 16A, pretreatment of the cells with TAS05567 reduced the levels of Syk phosphorylation in the presence of IgG, and its IC50 value was 25 nM. We also evaluated the inhibitory effects of TAS05567 on IgG-induced phosphorylation of BLNK, a downstream of Syk kinase. Pretreatment with TAS05567 dramatically decreased the levels of its phosphorylation in a concentration-dependent manner and the IC50 value was 9.7 nM (Figure 16B). In comparison with TAS05567, R406 showed markedly weaker inhibition of IgG-induced BLNK phosphorylation in SU-DHL-10 cells, similar to the results using Ramos cells, another B cell line. (IC50, 380 nM; data not shown). We further assessed the effectiveness of TAS05567 against expression of EGR2, which was identified as a downstream gene regulated by the BCR pathway [95]. TAS05567 strongly suppressed EGR2 gene expression in SU-DHL-10 cells (Figure 16C), which was comparable to the

inhibition observed in the assay for Syk activity.

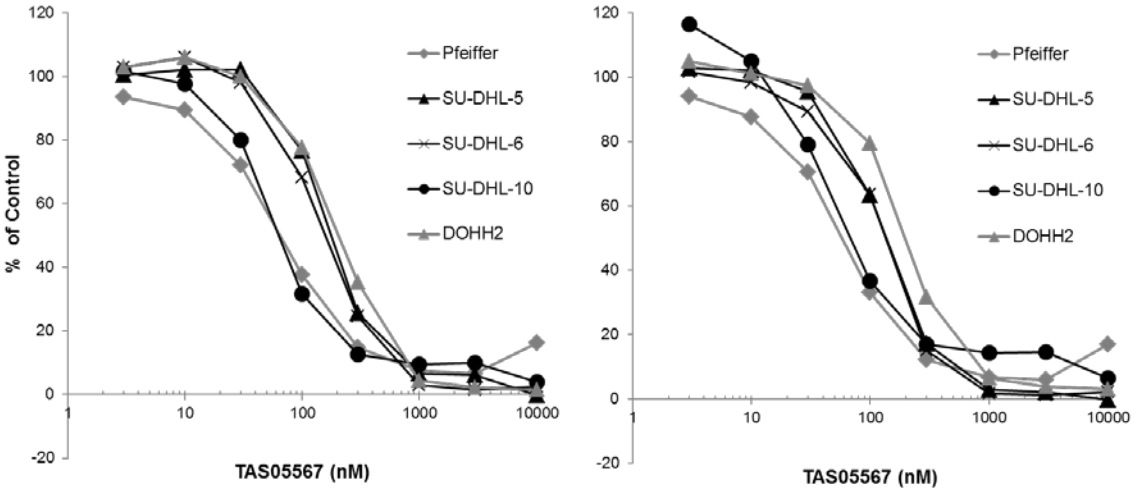

Figure 14. TAS05567 exhibits broad antiproliferative activity across various DLBCL cell lines *in vitro*.

DLBCL cell lines were treated with various concentrations of TAS05567 for 72 h. Cellular proliferation was determined via ATP quantification using the Cell Titer Glo assay. The same experiments were performed twice. Left graph shows the results of 1st experiment and right graph shows the results of 2nd experiment, respectively. Values are presented as percent of mean fluorescence intensity relative to vehicle control cells (100%) and non-stimulated control cells (0%). Data are presented as mean.

Table 7. IC50 values of DLBCL cell lines for TAS05567.

Cell	IC_{50} (nM)	
	1st	2nd
SU-DHL-5	180	130
SU-DHL-6	160	130
SU-DHL-10	69	80
DOHH2	210	210
Pfeiffer	67	59

Values are mean for the IC_{50} values.

The same experiments were performed twice. 1st indicates first experiment and 2nd indicates second experiment, respectively.

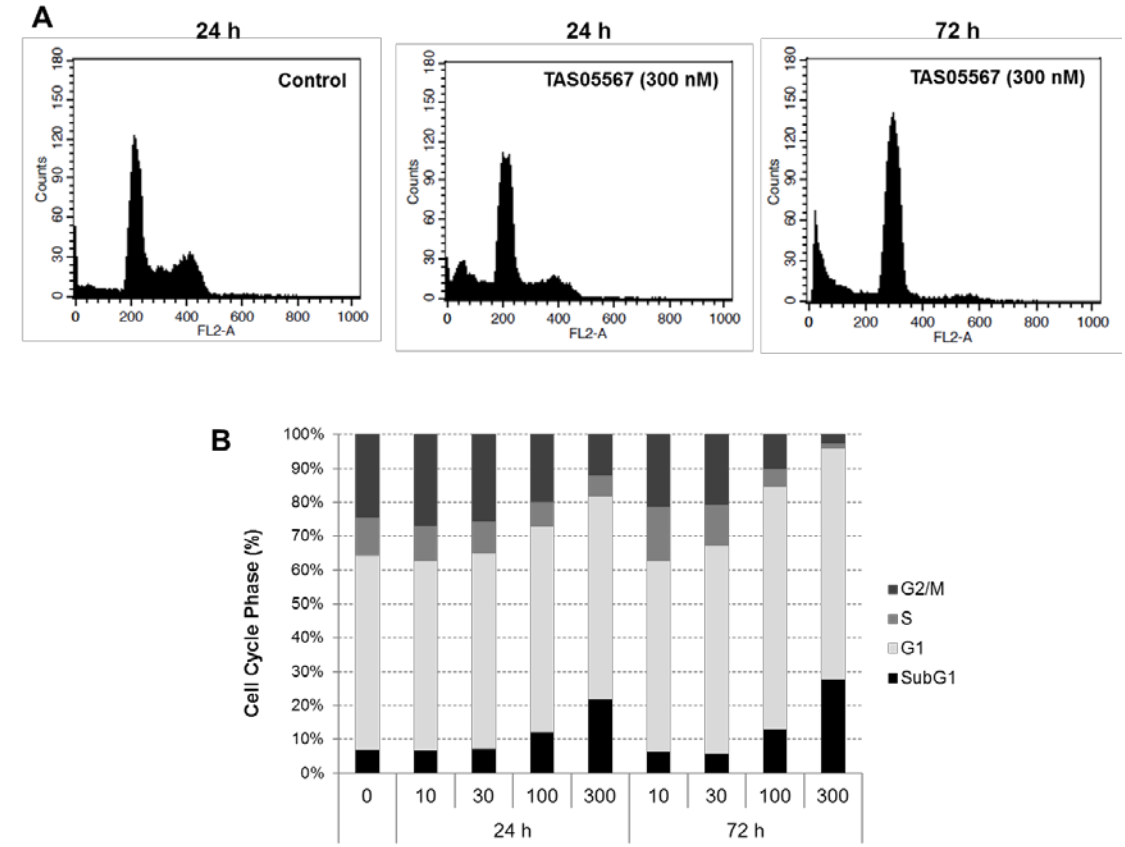

Figure 15. TAS5567 increases the percentages of cells in G1 phase and sub-G1 phase in a concentration-dependent manner.

(A) Representative histograms of cell cycle analysis at 24 h or 72 h incubation. SU-DHL-10 cells were treated with different concentrations of TAS05567 for 24 h or 72 h and cell cycle progression was examined by flow cytometer. Propidium iodide-labelled nuclei were analyzed for DNA content. (B) The bar diagram shows the percentage cell populations in the sub-G1 apoptotic population as well as the G1, S and G2/M phase populations of TAS05567 treated SU-DHL-10 cells. Analysis of cell number % of each cell cycle phase relative to total phases.

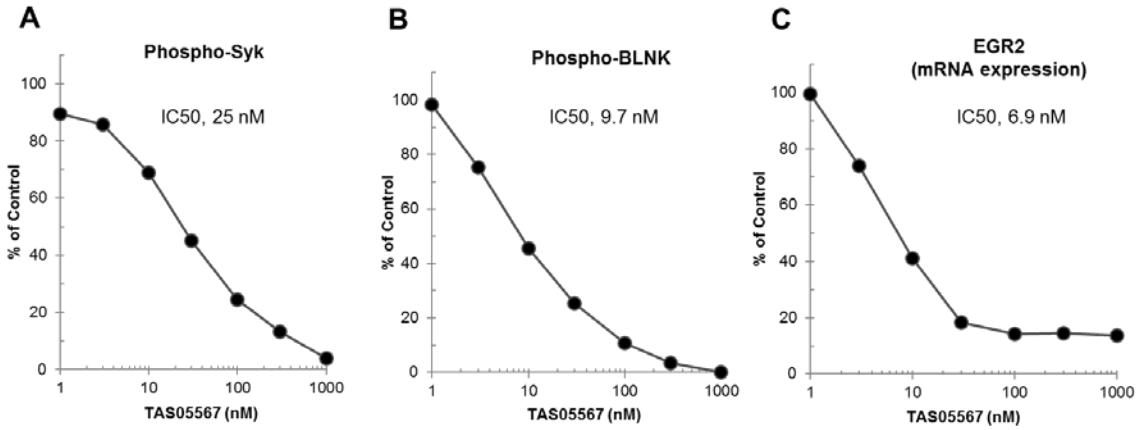

Figure 16. TAS5567 blocks BCR-mediated signaling cascades in SU-DHL-10 cells.

SU-DHL-10 cells were activated with anti-human IgG antibody for 10 min in the presence of increasing concentrations of TAS05567. The phosphorylation levels of Syk were analyzed by ELISA (A) and the phosphorylation levels of BLNK were analyzed by flow cytometry. (C) SU-DHL-10 cells were treated with different concentrations of TAS05567 for 8 h. The reaction of RT-PCR was performed using the 7900HT Fast Real-time PCR System. Gene expression profiling was performed using the comparative CT method for relative quantification. The calibration samples were untreated cells, and 18S rRNA was used as an endogenous control. Data are presented as mean.

2.3.4 TAS-5567 exhibits antitumor activity in SU-DHL-10 xenograft models without body weight loss

Next, to verify the *in vivo* antitumor activity of TAS05567 in the animal model, SU-DHL-10 cells were injected into the subcutaneous tissue of SCID mice. When the tumor volume reached approximately 200 mm^3, mice were randomized into three groups, and then 12.5 or 25 mg/kg/day of TAS05567 was orally administered for 14 days twice daily to the mice. TAS05567 (25 mg/kg) was associated with 62% inhibition of tumor growth compared with vehicle-treated mice at day15 (Figure 17A). Tumors from TAS05567 (25 mg/kg)-treated mice weighed significantly less than those from vehicle-treated mice, whereas low-dose with TAS05567 did not show significant effects (Figure 17B). No significant effects on body weight (Figure 17C) or signs of toxicity were observed in any of the treatment groups.

To determine the ability of TAS05567 to penetrate the tumor and exert its inhibitory activity against the Syk-mediated signaling pathway *in vivo*, we examined the pharmacodynamics of TAS05567 in SU-DHL-10 xenograft model. Phosphorylation of BLNK (Y84) in SU-DHL-10 tumors was detected following oral administration of vehicle or TAS05567 at effective dose (25 mg/kg). A single dose of TAS05567 resulted in approximately 95% inhibition observed at 6 h post dose (Figure 18A). Even at 18 h

post-second administration (24 h post-first administration) of TAS05567, the levels of BLNK phosphorylation were decreased by approximately 75%. Therefore, the Syk-mediated signaling pathway within the tumors was assumed to be suppressed continuously by more than 75% by treatment dose and schedule in the present study. Consistent with the inhibitory effects on the BLNK phosphorylation, the expression levels of EGR2 gene were also decreased by more than 85% at 14 h after the second administration (20 h post-first administration) of TAS05567 (Figure 18B).

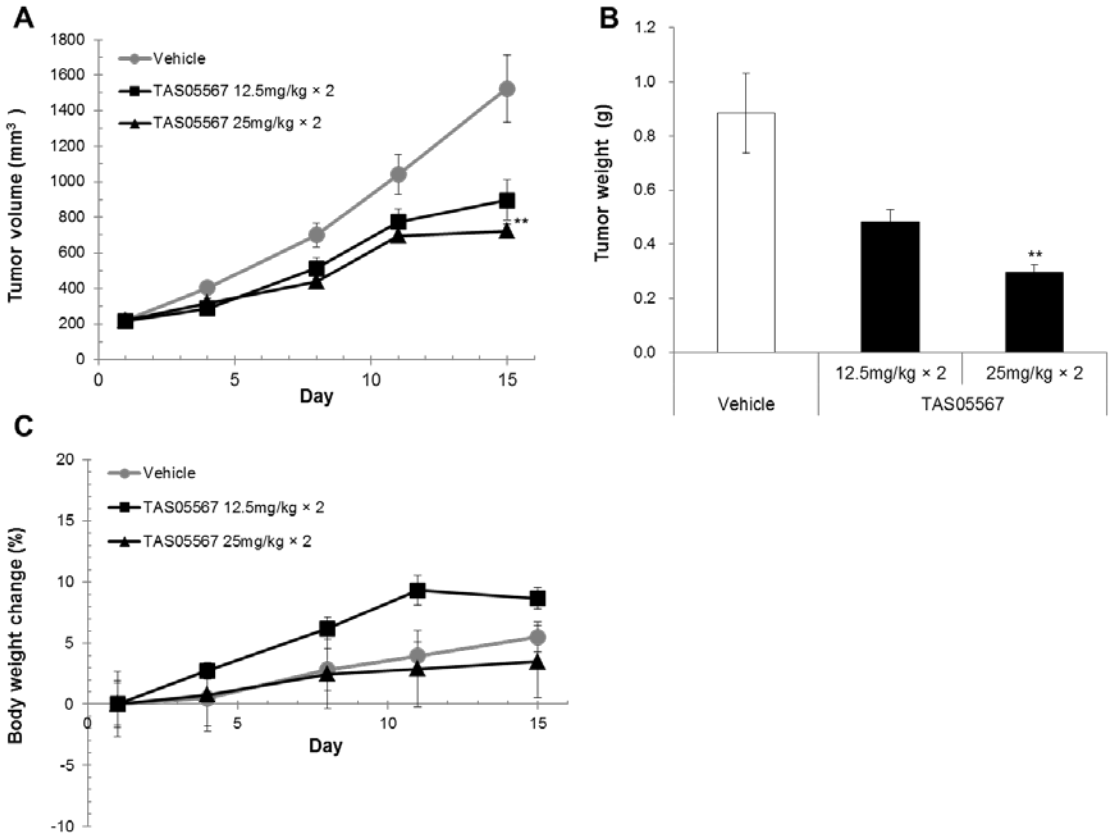

Figure 17. TAS05567 significantly reduces proliferation of SU-DHL-10 cells *in vivo*.

SU-DHL10 cells were implanted subcutaneously in SCID mice. Tumors were established to about 200 mm^3 in size before randomization in three groups for efficacy studies. Vehicle, TAS05567 (12.5 mg/kg) or TAS05567 (25 mg/kg) was then administered orally twice daily to mice for 14 days. TAS05567 slowed down tumor growth, as demonstrated by monitoring tumor volume change (A) and by measurement of tumor weight on day15 (B). As an indicator of toxicity, the mean of body weight change was calculated for each group (C). Data are presented as mean ± SEM (n=5 per group). ** $P<0.01$ compared with the vehicle group.

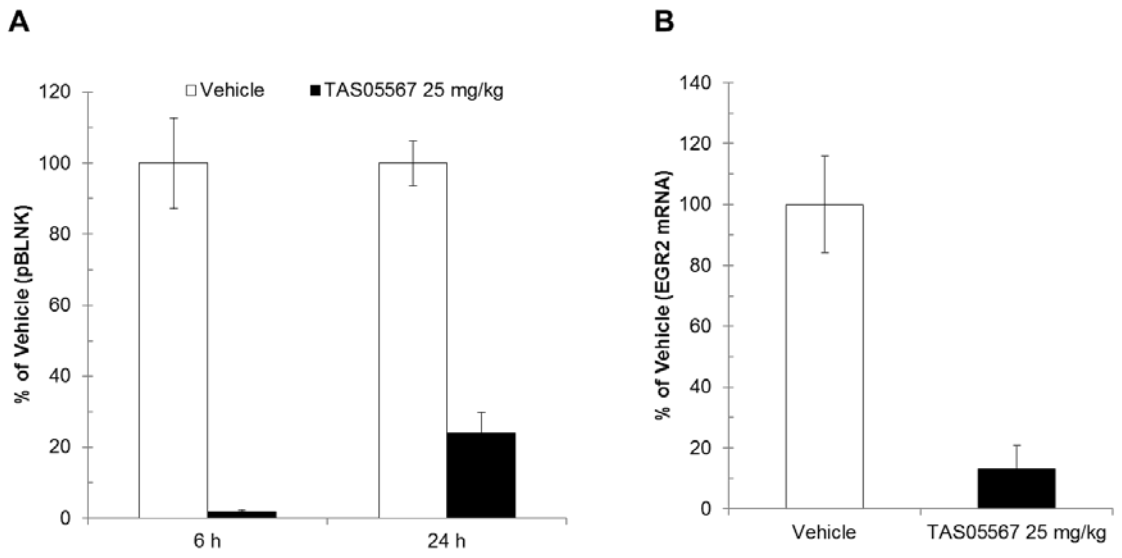

Figure 18. TAS05567 suppresses phosphorylation of BLNK and expression EGR2 gene in SU-DHL-10 tumors

Mice bearing established SU-DHL-10 tumors were treated with vehicle or TAS05567 (25 mg/kg) twice daily. The second administration was conducted at 6 h after the first administration. Tumors were collected at 6, 20, and 24 h after the administration of vehicle or TAS05567. (A) For analysis of phosphorylation of BLNK, the tumor tissues were dissociated, and then stimulated with anti-mouse IgG antibody for 10 min. The phosphorylation levels of BLNK in the suspended cells were analyzed by flow cytometry. Values are presented as percent of mean fluorescence intensity relative to vehicle-treated tumor cells stimulated with anti-IgM antibody (100%) and vehicle-treated tumor cells with no stimulation (0%). (B) For analysis of gene

expression, mRNA was extracted from the tumor tissues. The expression levels of EGR2 mRNA were determined by quantitative real-time PCR. The calibration samples were untreated cells, and 18S rRNA was used as an endogenous control. Values are presented as percent of mean EGR2 gene expression relative to vehicle-treated tumor cells (100%). Data are presented as mean ± SEM (n= 4 per group).

2.4 Discussion

We demonstrated that TAS05567 suppressed antigen-induced calcium flux as well as histamine release in IgE-sensitized basophilic cells. In addition, TAS05567 concentration-dependently inhibited cell proliferation of several DLBCL cell lines, and blocked Syk-mediated signaling pathway as well as cell cycle progression in SU-DHL-10 cells, which are highly sensitive to this compound. When TAS05567 orally was administered to TNP-IgE transgenic mice, the ear swelling induced was significantly suppressed in immediate phase after antigen exposure. Furthermore, TAS05567 significantly inhibited the tumor growth of mice with SU-DHL-10 xenograft and markedly reduced the levels of BLNK phosphorylation and EGR2 gene expression within the tumor tissues at effective dose, when compared to vehicle control.

Type 1 allergic diseases, including urticaria, asthma, and allergic rhinitis, are caused and exacerbated by IgE-mediated allergic reactions [28, 29]. Antigen-specific IgE bound to FcεRI on mast cells induces the release of chemical mediators such as histamine, causing the early symptoms of an allergic reaction [30]. Therefore, the symptoms of type 1 allergic diseases are typically alleviated with antihistamine drugs. As Syk acts upstream of signaling cascades induced by IgE cross-linking, TAS05567 potently inhibited the antigen/IgE-triggered intracellular calcium flux as well as

histamine release *in vitro* (Figure 12A and 12B). We further demonstrated the ability of TAS05567 to suppress immediate IgE-mediated allergic reactions *in vivo* using TNP-specific IgE transgenic mice. Unexpectedly, TAS05567 did not show a significant response in the late phase. One possible reason might not be enough concentration of TAS05567 to suppress the inflammation in this phase because its concentration at 24 h after the administration was lower than IC50 value of the whole blood assay even at 25 mg/kg (data not shown). Another possible reason is that IgE-mediated chemical mediator secretion through Syk activation contributes to the immediate allergic response, but the delayed response might depend on other signaling cascades (e.g., T-cell receptor signaling). Indeed, the immediate ear swelling caused by epicutaneous antigen challenge in this mouse model can be attributed primarily to a series of chemical mediators, including histamine, and thus, administration of an antihistamine inhibitor blocks the allergic response within a few hours post–antigen challenge. However, the antihistamine agent does not improve symptoms in the late phase, whereas cyclosporine A markedly inhibits ear swelling only in this phase [96]. As regards inhibition of immediate allergic responses, TAS05567 might be more potent than conventional drugs that target a single chemical mediator because Syk inhibition concomitantly suppresses secretion of multiple factors from mast cells, including histamine, arachidonate

metabolites, and cytokines [97]. From these findings, we expect that combination therapies including TAS05567 and inhibitors targeting T-cell function, such as cyclosporine A, will prove highly efficacious in the treatment of type I allergic diseases.

Since chronic activation of BCR signaling pathway has been reported to be implicated in the pathogenesis of a variety of B-cell malignancies, such as DLBCL, Syk kinases is expected to be an attractive drug target for therapy of these malignancies [41, 42]. In the present study, we first evaluated the inhibitory effects of TAS05567 on the cell proliferation using 5 cell lines of DLBLC *in vitro*, because DLBCL is generally and clinically considered a heterogeneous collection of malignancies [98]. Here, we demonstrated that TAS05567 suppressed the cell proliferation of all the cell lines in a concentration-dependent manner (Figure 14). Based on the cell-of-origin subtypes, DLBCL are further divided into germinal center B-cell (GCB) and non-GCB activated B-cell subtypes (ABC), with nearly 50% of cases being classified as the former subtype [99, 100]. All of the DLBCL cell lines we used were GCB subtype cells, as these cells are commercially available products. In general, ABC DLBCL is associated with considerably worse outcomes when treated with standard therapy (R-CHOP) and an inferior prognosis than GCB DLBCL [101, 102]. However, according to a report by Cheng et al., the effectiveness of Syk inhibitors against DLBCL cell lines of ABC

subtype has not seemed to be weaker than that against the cell lines of DLBCL subtype [42]. Hence, to clarify the possibility of TAS05567 as a therapeutic drug for patients suffering from DLBCL, we need further study to evaluate the inhibitory effects of TAS05567 on the proliferation of ABC DLBCL cells, such as HBL-1 or SU-DHL-2. Moreover, we examined a molecular mechanism underlying the effects of TAS05567 against the proliferation of SU-DHL-10 cells *in vitro*. TAS05567 not only decreased the levels of phosphorylation of Syk and BLNK as well as gene expression of EGR2, a factor regulated by BCR pathway, but also arrested cell cycle progression in the G1 phase, suggesting that these may cause repression of the proliferation of the cells.

In the *in vivo* antitumor activity study using SU-DHL-10 tumor-bearing mice, TAS05567 was orally administered twice daily at 12.5 mg/kg or 25 mg/kg to the mice for 14 days. While TAS05567 at 25 mg/kg showed a statistically significant tumor growth inhibition on day 15, treatment with low dose of TAS05567 exhibited a moderate inhibitory effect on the tumor growth and did not reach statistically significant (Figure 17A and 17B). The above data were unexpected, because TAS05567 ameliorated the symptoms in models of RA and ITP at less than 12.5 mg/kg. We are speculating on two possibilities why TAS05567 had a different response between anti-inflammatory effect and anti-tumor activity *in vivo*. One possible cause is that

tumor microenvironment may influence the antitumor activity of TAS05567 and the growth of subcutaneous SU-DHL-10 tumors in mice. The tumor microenvironment consists of a variety of stromal cells, endothelial cells, extracellular matrix, immune regulatory cells, growth factors, and cytokines that interact with cancer cells, which contributes to treatment resistance and tumor progression [103, 104]. In the present study, the immune regulatory cells, such as regulatory T cells, may have little influence on the tumor progression because of the use of severe immune deficient mice. However, the stromal cells and endothelial cells within the SU-DHL-10 tumors can produce growth factors and angiogenic factors cause accelerated neoangiogenesis and tumor progression, which may result in the attenuation of the antitumor efficacy by treatment of TAS05567. We suppose that the antitumor activity of TAS05567 may not be markedly enhanced by increasing the dose (> 25 mg/kg) or the frequency (three times daily) of our compound, because the level of BLNK phosphorylation within the tumor was already decreased by over 75% after 24 h of TAS05567 treatment at 25 mg/kg twice per day. Therefore, TAS05567 alone may fail to achieve complete tumor regression *in vivo*. R-CHOP rituximab, cyclophosphamide, doxorubicin, vincristine, prednisone) remains the standard of care for newly diagnosed DLBCL due to limited therapeutic options, even though approximately 30 to 40 % of patients develop relapsed

or refractory disease [90, 105, 106]. Now, we are investigating the effects of TAS05567 in combination with vincristine, doxorubicin, or prednisolone on the tumor growth *in vitro* as well as *in vivo*, and appropriate combination therapeutic strategies considering efficacy and safety will be determined in the future. The other possible cause is that we used the subcutaneous xenograft model in our experiment. Considering the origin of SU-DHL-10, a human B-cell malignant cell line, we should establish an orthotopic SU-DHL-10 xenograft model in mice, but we could not do that technically. In general, the hematopoietic cell microenvironment, including bone marrow stromal cells and resident macrophages, affects the growth and survival of lymphoma cells [107]. The growth rate of SU-DHL-10 cells *in vivo* may be difference between subcutaneously transplanted tumors and orthotopically transplanted tumors, because these tumor-supportive environments are not same. Recently, some orthotopic xenograft models have been established by transplanting lymphoma cells into hematopoietic organs, such as spleen, or intravenously into the irradiated mice [108, 109]. Therefore, we are currently developing an orthotopic transplantation model of SU-DHL-10 cells in mice, and will plan to evaluate the antitumor efficacy of TAS05567 using the orthotopic xenograft model.

Taken together, these results in this chapter suggest that TAS05567 may be a

promising new therapeutic option for patients with type 1 allergic diseases, such as atopic dermatitis, as well as B-cell malignancies, such as DLBCL.

Conclusion

In the present research, the pharmacological characteristics of TAS05567, a novel inhibitor of Syk kinase, were investigated for the purpose of developing a new therapeutic agent for the treatment of autoimmune and type 1 allergic diseases, and B-cell malignancies.

In Chapter 1, we first examined the potency and selectivity for kinases, receptors, channels, Ig-mediated intracellular, and cellular functional activity of TAS05567 by *in vitro* experiments using R406 as a comparison agent. TAS05567 potently inhibited Syk enzymatic activity with IC50 values of 0.37 nM (ATP concentration at Km level) and 1.5 nM (ATP concentration at the cellular level), but it only showed >70% inhibition of Syk and 4 other kinases among 192 kinases at 50 nM. In addition, TAS05567 showed at least 10-fold selectivity for Syk over JAK2, VEGFR2, FLT3, and RET, but R406 showed equal or greater efficacy against these kinases. TAS05567 only inhibited 1 of the 68 non-kinase targets tested at 10μM. Cell-based assays revealed that TAS05567 exhibited stronger inhibition of the IgM-induced phosphorylation of BLNK, PLCγ2, and Erk1/2 in B cells compared to R406. Moreover, FcγR-mediated TNF-α production as well as phagocytic activity, and mature osteoclast differentiation from precursor cells

were inhibited by treatment of TAS05567 in a concentration-dependent manner. As good absorption of TAS05567 was observed in both mice and rats following single dose oral administration of it, the *in vivo* efficacy of TAS05567 was evaluated in preclinical animal models of RA as well as ITP. The dose of TAS05567 for the *in vivo* experiments was estimated from the integration of the whole-blood assay data with single-dose pharmacokinetic data. When given prophylactically to mice with CAIA and mice with CIA, TAS05567 showed clear dose-dependent anti-inflammatory effects. Treatment with TAS05567 (> 10 mg/kg) or R406 resulted in a significantly reduction of paw volume and attenuated cartilage damage as well as bone destruction in rats with CIA when compared with the vehicle control despite the therapeutic regimen. Of note, while TAS05567 did not significantly change the red blood cell count or hemoglobin level in any dose group, R406 showed a statistically significant both parameters. Furthermore, both TAS05567 and R406 provided a significant protection against thrombocytopenia induced by anti-CD41 antibody in mice. However, when administered at 100 mg/kg, TAS05567 completely prevented thrombocytopenia, whereas R406 only partially prevented it. Based on these findings, TAS05567 would provide a better balance between efficacy and safety than R406 as a novel therapy for the treatment of autoimmune diseases.

In Chapter 2, we examined the effectiveness of TAS05567 on non-autoimmune diseases, including type 1 allergic diseases and DLBCL, caused by aberrant Ig production or BCR signaling cascade are involved in the pathogenesis. TAS05567 blocked the IgE receptor cross-linking-induced calcium flux and histamine release from basophilic cells. Besides the *in vitro* experiments, TAS05567 also suppressed the antigen-provoked ear swelling, a representative type 1 allergic reaction, in TNP-IgE transgenic mice at the same dosage that exhibited anti-inflammatory effects of it on autoimmune disease models. DLBCL, one of the B-cell malignancies, is mainly caused by chronic activation of BCR signaling pathway, and this disease is a heterogeneous both clinically and morphologically [41, 98, 110]. When we evaluated the inhibitory effects of TAS05567 on the cell proliferation using five cell lines of DLBCL, our compound showed good efficacy against the growth of all the cells. Additionally, treatment with TAS05567 resulted in the suppression of the phosphorylation levels of Syk and BLNK, the decrease of the expression of EGR2 mRNA, and the induction of cell cycle arrest in SU-DHL-10 cells. Further, TAS05567 significantly reduced the tumor growth of SU-DHL-10 xenografts in mice, although they received a higher total dose compared to the mice with inflammatory diseases. The BLNK phosphorylation and EGR2 gene expression within the tumor tissues were strongly inhibited following

treatment with TAS05567 at effective dose.

Currently, anti-TNF agents and JAK inhibitors as treatment for rheumatoid arthritis, and anti-IL-4 receptor antibody and calcineurin inhibitors as treatment for type 1 allergic diseases including atopic dermatitis have not only shown promising results in the clinical trials but also had superior efficacy to the conventional therapies in the real-world clinical practice. However, unfortunately, not all patients with above disorders benefit from these current treatment approaches, and therefore, many patients who do not shown a complete response to them have required new therapy options with a different spectrum of activity from the existing treatments. Since Syk is expressed in a variety of immune cells, such as B cells, macrophages, monocytes, mast cells, neutrophils, and osteoclasts, the inhibitors of Syk may exert a potent anti-inflammatory action in various diseases by different mechanisms from JAK inhibitors or calcineurin inhibitors mainly targeting the activated T cells. Furthermore, as TAS05567 is expected to be well tolerated due to highly selective blockade of Syk activity, the combination therapy of our compound and the existing drugs, including JAK inhibitors or tacrolimus, may offer great benefit for patients with RA or type 1 allergic diseases who fail the conventional therapies. In 2018, for the first time as an inhibitor of Syk kinase, Fostamatinib was approved by FDA as a therapeutic drug for patients with chronic ITP

[111]. Nevertheless, according to the results of Phase 3 trials, more than half of the patients have not shown any satisfactory response to this drug, and several adverse events, such diarrhea, hypertension, nausea, and transaminase elevation were observed similarly to past phase 2 studies of ITP [55]. Consequently, novel Syk inhibitors like TAS05567 with highly selective and exquisitely potent anti-inflammatory properties are required as new ITP therapeutic interventions. DLBCL is the most common NHL, accounting for 30–40% of NHL cases [112]. While R-CHOP is the current first-line standard treatment for patients with DLBCL, nearly 40% of patients will relapse or refractory disease following the initial therapy, indicating the need for alternative treatment approaches the decrease the risk of recurrence. While other types of Syk inhibitors, such as Cerdulatinib, a Syk/JAK dula inhibitor, and TAK-659, a Syk/Flt3 dual inhibitor, have been developed for patients with DLBCL, they are concerned about the side effects related to their selectivity towards protein kinases except for Syk [92, 113, 114]. From the view point of the psychological and physiological conditions of patients who have received the prior combination chemotherapy, we believe that alternative drugs with fewer side effects are much desired. In that sense, TAS 05567, which is a highly selective inhibitor for Syk, is expected to be well tolerated and provide excellent efficacy in patients with DLBCL by using it alone or in combination

with R-CHOP therapy. Recently, Ibrutinib, an irreversible inhibitor targeting Bruton's tyrosine kinase (Btk), another downstream molecule of BCR signaling pathway, has shown significant clinical benefit in patients with B-cell malignancies, including DLBCL, follicular lymphoma (FL), and Waldenström's macroglobulinemia (WM) [115]. However, it has been reported that mutation of C481S in Btk resulted in loss of Ibrutinib binding and restoration of Btk activity in the presence of this drug, subsequent reactivation of BCR signaling, eventually leading to clinical relapse [116]. On the contrary, as Syk is thought to be activated upstream of Btk in the BCR signaling cascade [117], TAS05567 may provide a clinical benefit for patients with B-cell malignancies harboring Btk^{C481S} mutation through the blockade of Syk activity.

Taken together, in this study we demonstrate that TAS05567, a novel highly selective and potent inhibitor of Syk, would provide an effective therapy for a broad range of disorders, including autoimmune diseases, type 1 allergic diseases, and DLBCL. Considering the enormous results from the past clinical trials in which many patients have not shown substantial clinical benefit or fail to achieve complete remission in the above-mentioned diseases, alternative treatment strategies are urgently desired for these patients. We expect that our findings obtained by this study will lead to new treatment options for patients suffering from inflammatory diseases as well as B-cell

malignancies.

Acknowledgements

Firstly, my heartfelt appreciation goes to Prof. Yasuhiro Yasutomi (National Institutes of Biomedical Innovation, Health and Nutrition) whose comments and suggestions were of inestimable value for my research. I am also deeply grateful to Prof. Atsushi Yoshiki (Experimental Animal Division, RIKEN BioResource Center) and Prof. Toshikazu Kamiya (Research Fellow, Kyowa Hakko Bio Co., Ltd.) for reviewing my manuscript and giving insightful comments.

My sincere thanks and gratitude extend to Dr. Eiji Sasaki (Taiho Pharmaceutical Co., LTD.) for instructing me in all aspects about this research with unlimited patience, for his guidance, valuable suggestions and fruitful discussions about this research project.

I also greatly appreciate the help of Dr. Yoshio Ogino, Mr. Hiroki Irie, Ms. Naoko Fujino, and Mr. Takafumi Harada (Taiho Pharmaceutical Co., LTD.) for their kindness, guidance and support during my research work. I would like to thank Mr. Ryusuke Kaneko, Mr. Manabu Tayama, Mr. Shunsuke Demizu, and Mr. Daichi Akasaka (Taiho Pharmaceutical Co., LTD.) for their continuous support and patience with my research.

I appreciate the feedback offered by Dr. Fumihito Hosoi, Dr. Yohei Yoshiga, and Dr. Fumito Tatsuzawa of Taiho Pharmaceutical Co., LTD. during preparation for this

manuscript.

Finally, I would also like to express my gratitude to Eriko, Rikuto, Yusei, and Hayashi family for their moral support and warm encouragement.

References

1. Bach JF. The effect of infections on susceptibility to autoimmune and allergic diseases. The New England journal of medicine. 2002;347(12):911-20.

2. Eaton WW, Pedersen MG, Atladottir HO, Gregory PE, Rose NR, Mortensen PB. The prevalence of 30 ICD-10 autoimmune diseases in Denmark. Immunologic research. 2010;47(1-3):228-31.

3. Mackay IR, Leskovsek NV, Rose NR. The odd couple: a fresh look at autoimmunity and immunodeficiency. J Autoimmun. 2010;35(3):199-205.

4. Gabriel SE. The epidemiology of rheumatoid arthritis. Rheum Dis Clin North Am. 2001;27(2):269-81.

5. Parida JR, Misra DP, Wakhlu A, Agarwal V. Is non-biological treatment of rheumatoid arthritis as good as biologics? World journal of orthopedics. 2015;6(2):278-83.

6. Scott DL. Biologics-based therapy for the treatment of rheumatoid arthritis. Clin Pharmacol Ther. 2012;91(1):30-43.

7. Tanaka Y. Recent progress and perspective in JAK inhibitors for rheumatoid arthritis: from bench to bedside. Journal of biochemistry. 2015;158(3):173-9.

8. Wollenhaupt J, Silverfield J, Lee EB, Curtis JR, Wood SP, Soma K, et al. Safety and efficacy of tofacitinib, an oral janus kinase inhibitor, for the treatment of rheumatoid arthritis in open-label, longterm extension studies. The Journal of rheumatology. 2014;41(5):837-52.

9. Tan EM. Antinuclear antibodies: diagnostic markers for autoimmune diseases and probes for cell biology. Adv Immunol. 1989;44:93-151.

10. Suurmond J, Diamond B. Autoantibodies in systemic autoimmune diseases: specificity and pathogenicity. J Clin Invest. 2015;125(6):2194-202.

11. Treanor B. B-cell receptor: from resting state to activate. Immunology. 2012;136(1):21-7.

12. Guilliams M, Bruhns P, Saeys Y, Hammad H, Lambrecht BN. The function of Fcgamma receptors in dendritic cells and macrophages. Nat Rev Immunol. 2014;14(2):94-108.

13. van den Berg WB, van Riel PL. Uncoupling of inflammation and destruction in rheumatoid arthritis: myth or reality? Arthritis and rheumatism. 2005;52(4):995-9.

14. Leandro MJ, Cambridge G, Ehrenstein MR, Edwards JC. Reconstitution of peripheral blood B cells after depletion with rituximab in patients with rheumatoid arthritis. Arthritis and rheumatism. 2006;54(2):613-20.

15. Cohen MD, Keystone E. Rituximab for Rheumatoid Arthritis. Rheumatology and therapy. 2015;2(2):99-111.

16. Banda NK, Thurman JM, Kraus D, Wood A, Carroll MC, Arend WP, et al. Alternative complement pathway activation is essential for inflammation and joint destruction in the passive transfer model of collagen-induced arthritis. J Immunol. 2006;177(3):1904-12.

17. Kagari T, Tanaka D, Doi H, Shimozato T. Essential role of Fc gamma receptors in anti-type II collagen antibody-induced arthritis. J Immunol. 2003;170(8):4318-24.

18. Barnes N, Gavin AL, Tan PS, Mottram P, Koentgen F, Hogarth PM. FcgammaRI-deficient mice show multiple alterations to inflammatory and immune responses. Immunity. 2002;16(3):379-89.

19. Terrell DR, Beebe LA, Vesely SK, Neas BR, Segal JB, George JN. The incidence of immune thrombocytopenic purpura in children and adults: A critical review of published reports. Am J Hematol. 2010 Mar;85(3):174-80.

20. Kikuchi K, Miyakawa Y, Ikeda S, Sato Y, Takebayashi T. Cost-effectiveness of adding rituximab to splenectomy and romiplostim for treating steroid-resistant idiopathic thrombocytopenic purpura in adults. BMC Health Serv Res. 2015 Jan 22;15:2.

21. Crow AR, Lazarus AH. Role of Fcgamma receptors in the pathogenesis and treatment of idiopathic thrombocytopenic purpura. J Pediatr Hematol Oncol. 2003;25 Suppl 1:S14-8.

22. Shad AT, Gonzalez CE, Sandler SG. Treatment of immune thrombocytopenic purpura in children : current concepts. Paediatric drugs. 2005;7(5):325-36.

23. Arnold DM. Bleeding complications in immune thrombocytopenia. Hematology American Society of Hematology Education Program. 2015;2015:237-42.

24. Debre M, Bonnet MC, Fridman WH, Carosella E, Philippe N, Reinert P, et al. Infusion of Fc gamma fragments for treatment of children with acute immune thrombocytopenic purpura. Lancet. 1993;342(8877):945-9.

25. Neschadim A, Branch DR. Mouse Models for Immune-Mediated Platelet Destruction or Immune Thrombocytopenia (ITP). Curr Protoc Immunol. 2016;113:15 30 1-15 30 13.

26. Pawankar R. Allergic diseases and asthma: a global public health concern and a call to action. World Allergy Organ J. 2014 May 19;7(1):12.

27. Noval Rivas M, Chatila TA. Regulatory T cells in allergic diseases. J Allergy Clin Immunol. 2016 Sep;138(3):639-652.

28. Galli SJ, Tsai M. IgE and mast cells in allergic disease. Nature medicine.

2012;18(5):693-704.

29. Navines-Ferrer A, Serrano-Candelas E, Molina-Molina GJ, Martin M. IgE-Related Chronic Diseases and Anti-IgE-Based Treatments. Journal of immunology research. 2016;2016:8163803.

30. Stone KD, Prussin C, Metcalfe DD. IgE, mast cells, basophils, and eosinophils. The Journal of allergy and clinical immunology. 2010;125(2 Suppl 2):S73-80.

31. Taube C, Wei X, Swasey CH, Joetham A, Zarini S, Lively T, et al. Mast cells, Fc epsilon RI, and IL-13 are required for development of airway hyperresponsiveness after aerosolized allergen exposure in the absence of adjuvant. J Immunol. 2004;172(10):6398-406.

32. D'Amato G, Salzillo A, Piccolo A, D'Amato M, Liccardi G. A review of anti-IgE monoclonal antibody (omalizumab) as add on therapy for severe allergic (IgE-mediated) asthma. Therapeutics and clinical risk management. 2007;3(4):613-9.

33. Turner M, Schweighoffer E, Colucci F, Di Santo JP, Tybulewicz VL. Tyrosine kinase SYK: essential functions for immunoreceptor signalling. Immunol Today. 2000;21(3):148-54.

34. Mocsai A, Ruland J, Tybulewicz VL. The SYK tyrosine kinase: a crucial player in diverse biological functions. Nat Rev Immunol. 2010;10(6):387-402.

35. Deng GM, Kyttaris VC, Tsokos GC. Targeting Syk in Autoimmune Rheumatic Diseases. Frontiers in immunology. 2016;7:78.

36. Huang ZY, Kim MK, Kim-Han TH, Indik ZK, Schreiber AD. Effect of locally administered Syk siRNA on allergen-induced arthritis and asthma. Mol Immunol. 2013;53(1-2):52-9.

37. Jakus Z, Simon E, Balazs B, Mocsai A. Genetic deficiency of Syk protects mice from autoantibody-induced arthritis. Arthritis and rheumatism. 2010;62(7):1899-910.

38. Kiefer F, Brumell J, Al-Alawi N, Latour S, Cheng A, Veillette A, et al. The Syk protein tyrosine kinase is essential for Fcgamma receptor signaling in macrophages and neutrophils. Mol Cell Biol. 1998;18(7):4209-20.

39. Yamasaki T, Ariyoshi W, Okinaga T, Adachi Y, Hosokawa R, Mochizuki S, et al. The dectin 1 agonist curdlan regulates osteoclastogenesis by inhibiting nuclear factor of activated T cells cytoplasmic 1 (NFATc1) through Syk kinase. J Biol Chem. 2014;289(27):19191-203.

40. Costello PS, Turner M, Walters AE, Cunningham CN, Bauer PH, Downward J, et al. Critical role for the tyrosine kinase Syk in signalling through the high affinity IgE receptor of mast cells. Oncogene. 1996;13(12):2595-605.

41. Chen L, Monti S, Juszczynski P, Daley J, Chen W, Witzig TE, et al. SYK-dependent

tonic B-cell receptor signaling is a rational treatment target in diffuse large B-cell lymphoma. Blood. 2008;111(4):2230-7.

42. Cheng S, Coffey G, Zhang XH, Shaknovich R, Song Z, Lu P, et al. SYK inhibition and response prediction in diffuse large B-cell lymphoma. Blood. 2011;118(24):6342-52.

43. Crump M, Neelapu SS, Farooq U, Van Den Neste E, Kuruvilla J, Westin J, et al. Outcomes in refractory diffuse large B-cell lymphoma: results from the international SCHOLAR-1 study. Blood. 2017;130(16):1800-8.

44. Bajpai M. Fostamatinib, a Syk inhibitor prodrug for the treatment of inflammatory diseases. IDrugs. 2009;12(3):174-85.

45. Podolanczuk A, Lazarus AH, Crow AR, Grossbard E, Bussel JB. Of mice and men: an open-label pilot study for treatment of immune thrombocytopenic purpura by an inhibitor of Syk. Blood. 2009;113(14):3154-60.

46. Braselmann S, Taylor V, Zhao H, Wang S, Sylvain C, Baluom M, et al. R406, an orally available spleen tyrosine kinase inhibitor blocks fc receptor signaling and reduces immune complex-mediated inflammation. The Journal of pharmacology and experimental therapeutics. 2006;319(3):998-1008.

47. Ferguson GD, Delgado M, Plantevin-Krenitsky V, Jensen-Pergakes K, Bates RJ,

Torres S, et al. A Novel Triazolopyridine-Based Spleen Tyrosine Kinase Inhibitor That Arrests Joint Inflammation. PloS one. 2016;11(1):e0145705.

48. Burke RT, Meadows S, Loriaux MM, Currie KS, Mitchell SA, Maciejewski P, et al. A potential therapeutic strategy for chronic lymphocytic leukemia by combining Idelalisib and GS-9973, a novel spleen tyrosine kinase (Syk) inhibitor. Oncotarget. 2014;5(4):908-15.

49. Feldmann M, Brennan FM, Maini RN. Rheumatoid arthritis. Cell. 1996;85(3):307-10.

50. Goekoop-Ruiterman YP, Huizinga TW. Rheumatoid arthritis: can we achieve true drug-free remission in patients with RA? Nature reviews Rheumatology. 2010;6(2):68-70.

51. Firestein GS. Evolving concepts of rheumatoid arthritis. Nature. 2003;423(6937):356-61.

52. Chaiamnuay S, Bridges SL, Jr. The role of B cells and autoantibodies in rheumatoid arthritis. Pathophysiology : the official journal of the International Society for Pathophysiology. 2005;12(3):203-16.

53. Kaur M, Singh M, Silakari O. Inhibitors of switch kinase 'spleen tyrosine kinase' in inflammation and immune-mediated disorders: a review. European journal of medicinal

chemistry. 2013;67:434-46.

54. Pine PR, Chang B, Schoettler N, Banquerigo ML, Wang S, Lau A, et al. Inflammation and bone erosion are suppressed in models of rheumatoid arthritis following treatment with a novel Syk inhibitor. Clin Immunol. 2007;124(3):244-57.

55. Bussel J, Arnold DM, Grossbard E, Mayer J, Trelinski J, Homenda W, et al. Fostamatinib for the treatment of adult persistent and chronic immune thrombocytopenia: Results of two phase 3, randomized, placebo-controlled trials. American journal of hematology. 2018;93(7):921-30.

56. Weinblatt ME, Kavanaugh A, Burgos-Vargas R, Dikranian AH, Medrano-Ramirez G, Morales-Torres JL, et al. Treatment of rheumatoid arthritis with a Syk kinase inhibitor: a twelve-week, randomized, placebo-controlled trial. Arthritis and rheumatism. 2008;58(11):3309-18.

57. Hayman SR, Leung N, Grande JP, Garovic VD. VEGF inhibition, hypertension, and renal toxicity. Current oncology reports. 2012;14(4):285-94.

58. Verstovsek S. Therapeutic potential of Janus-activated kinase-2 inhibitors for the management of myelofibrosis. Clinical cancer research : an official journal of the American Association for Cancer Research. 2010;16(7):1988-96.

59. Lengel D, Lamm Bergstrom E, Barthlow H, Oldman K, Musgrove H, Harmer A, et

al. Prevention of fostamatinib-induced blood pressure elevation by antihypertensive agents. Pharmacology research & perspectives. 2015;3(5):e00176.

60. Friedberg JW, Sharman J, Sweetenham J, Johnston PB, Vose JM, Lacasce A, et al. Inhibition of Syk with fostamatinib disodium has significant clinical activity in non-Hodgkin lymphoma and chronic lymphocytic leukemia. Blood. 2010;115(13):2578-85.

61. McAdoo SP, Tam FW. Fostamatinib Disodium. Drugs of the future. 2011;36(4):273.

62. Vogelpoel LT, Baeten DL, de Jong EC, den Dunnen J. Control of cytokine production by human fc gamma receptors: implications for pathogen defense and autoimmunity. Frontiers in immunology. 2015;6:79.

63. Liao C, Hsu J, Kim Y, Hu DQ, Xu D, Zhang J, et al. Selective inhibition of spleen tyrosine kinase (SYK) with a novel orally bioavailable small molecule inhibitor, RO9021, impinges on various innate and adaptive immune responses: implications for SYK inhibitors in autoimmune disease therapy. Arthritis research & therapy. 2013;15(5):R146.

64. Lin YC, Huang DY, Wang JS, Lin YL, Hsieh SL, Huang KC, et al. Syk is involved in NLRP3 inflammasome-mediated caspase-1 activation through adaptor ASC phosphorylation and enhanced oligomerization. Journal of leukocyte biology.

2015;97(5):825-35.

65. Nandakumar KS, Andren M, Martinsson P, Bajtner E, Hellstrom S, Holmdahl R, et al. Induction of arthritis by single monoclonal IgG anti-collagen type II antibodies and enhancement of arthritis in mice lacking inhibitory FcgammaRIIB. Eur J Immunol. 2003;33(8):2269-77.

66. Joe B, Griffiths MM, Remmers EF, Wilder RL. Animal models of rheumatoid arthritis and related inflammation. Current rheumatology reports. 1999;1(2):139-48.

67. Joosten LA, Lubberts E, Helsen MM, Saxne T, Coenen-de Roo CJ, Heinegard D, et al. Protection against cartilage and bone destruction by systemic interleukin-4 treatment in established murine type II collagen-induced arthritis. Arthritis research. 1999;1(1):81-91.

68. Sonbol MB, Firwana B, Zarzour A, Morad M, Rana V, Tiu RV. Comprehensive review of JAK inhibitors in myeloproliferative neoplasms. Therapeutic advances in hematology. 2013;4(1):15-35.

69. Lundquist LM, Cole SW, Sikes ML. Efficacy and safety of tofacitinib for treatment of rheumatoid arthritis. World journal of orthopedics. 2014;5(4):504-11.

70. Zhang X, Chua L, Ernest C, 2nd, Macias W, Rooney T, Tham LS. Dose/Exposure-Response Modeling to Support Dosing Recommendation for Phase III

Development of Baricitinib in Patients with Rheumatoid Arthritis. CPT: pharmacometrics & systems pharmacology. 2017;6(12):804-13.

71. Matsuura M. Structural Modifications of Bacterial Lipopolysaccharide that Facilitate Gram-Negative Bacteria Evasion of Host Innate Immunity. Frontiers in immunology. 2013;4:109.

72. Tan Sardjono C, Mottram PL, Hogarth PM. The role of FcgammaRIIa as an inflammatory mediator in rheumatoid arthritis and systemic lupus erythematosus. Immunology and cell biology. 2003;81(5):374-81.

73. Burkhardt H, Koller T, Engstrom A, Nandakumar KS, Turnay J, Kraetsch HG, et al. Epitope-specific recognition of type II collagen by rheumatoid arthritis antibodies is shared with recognition by antibodies that are arthritogenic in collagen-induced arthritis in the mouse. Arthritis and rheumatism. 2002;46(9):2339-48.

74. Coffey G, DeGuzman F, Inagaki M, Pak Y, Delaney SM, Ives D, et al. Specific inhibition of spleen tyrosine kinase suppresses leukocyte immune function and inflammation in animal models of rheumatoid arthritis. The Journal of pharmacology and experimental therapeutics. 2012;340(2):350-9.

75. Kremlitzka M, Macsik-Valent B, Erdei A. Syk is indispensable for CpG-induced activation and differentiation of human B cells. Cellular and molecular life sciences :

CMLS. 2015;72(11):2223-36.

76. Kim JY, Park SH, Baek JM, Erkhembaatar M, Kim MS, Yoon KH, et al. Harpagoside Inhibits RANKL-Induced Osteoclastogenesis via Syk-Btk-PLCgamma2-Ca(2+) Signaling Pathway and Prevents Inflammation-Mediated Bone Loss. Journal of natural products. 2015;78(9):2167-74.

77. Takeuchi T, Tanaka Y, Ishiguro N, Yamanaka H, Yoneda T, Ohira T, et al. Effect of denosumab on Japanese patients with rheumatoid arthritis: a dose-response study of AMG 162 (Denosumab) in patients with RheumatoId arthritis on methotrexate to Validate inhibitory effect on bone Erosion (DRIVE)-a 12-month, multicentre, randomised, double-blind, placebo-controlled, phase II clinical trial. Annals of the rheumatic diseases. 2016;75(6):983-90.

78. Tseng S, Reddi AH, Di Cesare PE. Cartilage Oligomeric Matrix Protein (COMP): A Biomarker of Arthritis. Biomarker insights. 2009;4:33-44.

79. Kelley MJ, Rose AY, Song K, Chen Y, Bradley JM, Rookhuizen D, et al. Synergism of TNF and IL-1 in the induction of matrix metalloproteinase-3 in trabecular meshwork. Investigative ophthalmology & visual science. 2007;48(6):2634-43.

80. Cha HS, Boyle DL, Inoue T, Schoot R, Tak PP, Pine P, et al. A novel spleen tyrosine kinase inhibitor blocks c-Jun N-terminal kinase-mediated gene expression in

synoviocytes. The Journal of pharmacology and experimental therapeutics. 2006;317(2):571-8.

81. Lu Y, Wang W, Mao H, Hu H, Wu Y, Chen BG, et al. Antibody-mediated platelet phagocytosis by human macrophages is inhibited by siRNA specific for sequences in the SH2 tyrosine kinase, Syk. Cellular immunology. 2011;268(1):1-3.

82. Ozaki E, Campbell M, Doyle SL. Targeting the NLRP3 inflammasome in chronic inflammatory diseases: current perspectives. Journal of inflammation research. 2015;8:15-27.

83. Dinarello CA, Simon A, van der Meer JW. Treating inflammation by blocking interleukin-1 in a broad spectrum of diseases. Nature reviews Drug discovery. 2012;11(8):633-52.

84. Pawankar R, Baena-Cagnani CE, Bousquet J, Canonica GW, Cruz AA, Kaliner MA, et al. State of world allergy report 2008: allergy and chronic respiratory diseases. The World Allergy Organization journal. 2008;1(6 Suppl):S4-S17.

85. HayGlass KT. Allergy: who, why and what to do about it? Immunol Today. 1995;16(11):505-7.

86. De Martinis M, Sirufo MM, Ginaldi L. Allergy and Aging: An Old/New Emerging Health Issue. Aging and disease. 2017;8(2):162-75.

87. Flowers CR, Sinha R, Vose JM. Improving outcomes for patients with diffuse large B-cell lymphoma. CA Cancer J Clin. 2010;60(6):393–408.

88. Sant M, Allemani C, Tereanu C, et al. Incidence of hematologic malignancies in Europe by morphologic subtype: results of the HAEMACARE project. Blood. 2010;116(19):3724–34.

89. Morton LM, Wang SS, Devesa SS, Hartge P, Weisenburger DD, Linet MS. Lymphoma incidence patterns by WHO subtype in the United States, 1992–2001. Blood. 2006;107(1):265–276.

90. Coiffier B, Lepage E, Briere J, Herbrecht R, Tilly H, Bouabdallah R, et al. CHOP chemotherapy plus rituximab compared with CHOP alone in elderly patients with diffuse large-B-cell lymphoma. The New England journal of medicine. 2002;346(4):235-42.

91. Coiffier B, Sarkozy C. Diffuse large B-cell lymphoma: R-CHOP failure-what to do? Hematology American Society of Hematology Education Program. 2016;2016(1):366-78.

92. Liu D, Mamorska-Dyga A. Syk inhibitors in clinical development for hematological malignancies. Journal of hematology & oncology. 2017;10(1):145.

93. J. Kurebayashi, M. Nukatsuka, H. Sonoo, J. Uchida, M. Kiniwa M, Preclinical

rationale for combined use of endocrine therapy and 5-fluorouracil but neither doxorubicin nor paclitaxel in the treatment of endocrine-responsive breast cancer, Cancer Chemother. Pharmacol. 2010;65:219–25.

94. Wex E, Bouyssou T, Duechs MJ, Erb KJ, Gantner F, Sanderson MP, et al. Induced Syk deletion leads to suppressed allergic responses but has no effect on neutrophil or monocyte migration in vivo. Eur J Immunol. 2011;41(11):3208-18.

95. Krysiak K, Gomez F, White BS, Matlock M, Miller CA, Trani L, et al. Recurrent somatic mutations affecting B-cell receptor signaling pathway genes in follicular lymphoma. Blood. 2017;129(4):473-83.

96. Sato E, Hirahara K, Wada Y, Yoshitomi T, Azuma T, Matsuoka K, et al. Chronic inflammation of the skin can be induced in IgE transgenic mice by means of a single challenge of multivalent antigen. The Journal of allergy and clinical immunology. 2003;111(1):143-8.

97. Kato T, Iwasaki H, Kobayashi H, Miyagawa N, Matsuo A, Hata T, et al. JTE-852, a novel spleen tyrosine kinase inhibitor, blocks mediator secretion from mast cells with immunoglobulin E crosslinking. European journal of pharmacology. 2017;801:1-8.

98. Friedberg JW, Fisher RI. Diffuse large B-cell lymphoma. Hematol Oncol Clin North Am. 2008;22(5):941-52.

99. Li S, Young KH, Medeiros LJ. Diffuse large B-cell lymphoma. Pathology. 2018;50(1):74-87.

100. Barton S, Hawkes EA, Wotherspoon A, Cunningham D. Are we ready to stratify treatment for diffuse large B-cell lymphoma using molecular hallmarks? The oncologist. 2012;17(12):1562-73.

101. Vaidya R, Witzig TE. Prognostic factors for diffuse large B-cell lymphoma in the R(X)CHOP era. Annals of oncology : official journal of the European Society for Medical Oncology. 2014;25(11):2124-33.

102. Nowakowski GS, Czuczman MS. ABC, GCB, and Double-Hit Diffuse Large B-Cell Lymphoma: Does Subtype Make a Difference in Therapy Selection? American Society of Clinical Oncology educational book American Society of Clinical Oncology Meeting. 2015:e449-57.

103. Gould CM, Courtneidge SA. Regulation of invadopodia by the tumor microenvironment. Cell adhesion & migration. 2014;8(3):226-35.

104. Ahn DH, Ramanathan RK, Bekaii-Saab T. Emerging Therapies and Future Directions in Targeting the Tumor Stroma and Immune System in the Treatment of Pancreatic Adenocarcinoma. Cancers. 2018;10(6):193.

105. Martelli M, Ferreri AJ, Agostinelli C, Di Rocco A, Pfreundschuh M, Pileri SA.

Diffuse large B-cell lymphoma. Crit Rev Oncol Hematol. 2013;87(2):146-71.

106. Sehn LH. Paramount prognostic factors that guide therapeutic strategies in diffuse large B-cell lymphoma. Hematology Am Soc Hematol Educ Program. 2012;2012:402-9.

107. Fecteau JF, Kipps TJ. Structure and function of the hematopoietic cancer niche: focus on chronic lymphocytic leukemia. Front Biosci (Schol Ed). 2012;4:61-73.

108. Matsumoto T, Suetsugu A, Hasegawa K, Nakamura M, Aoki H, Kunisada T, et al. Color-Coded Imaging of Syngeneic Orthotopic Malignant Lymphoma Interacting with Host Stromal Cells During Metastasis. Anticancer research. 2016;36(4):1473-8.

109. Kohnken R, Porcu P, Mishra A. Overview of the Use of Murine Models in Leukemia and Lymphoma Research. Front Oncol. 2017; 7: 22.

110. Staudt LM, Dave S. The biology of human lymphoid malignancies revealed by gene expression profiling. Advances in immunology. 2005;87:163-208.

111. FDA approves fostamatinib tablets for ITP. U.S. Food and Drug Administration Web site. http://www fda.gov/drugs/informationondrugs/approveddrugs/ucm604956.htmUpdated April 28, 2018. Accessed August 28, 2018.

112. Wang ES, Teruya-Feldstein J, Wu Y, Zhu Z, Hicklin DJ, Moore MA. Targeting autocrine and paracrine VEGF receptor pathways inhibits human lymphoma xenografts

in vivo. Blood. 2004;104(9):2893-902.

113. Lam B, Arikawa Y, Cramlett J, Dong Q, de Jong R, Feher V, et al. Discovery of TAK-659 an orally available investigational inhibitor of Spleen Tyrosine Kinase (SYK). Bioorganic & medicinal chemistry letters. 2016;26(24):5947-50.

114. Guo A, Lu P, Coffey G, Conley P, Pandey A, Wang YL. Dual SYK/JAK inhibition overcomes ibrutinib resistance in chronic lymphocytic leukemia: Cerdulatinib, but not ibrutinib, induces apoptosis of tumor cells protected by the microenvironment. Oncotarget. 2017;8(8):12953-67.

115. Wang Y, Zhang LL, Champlin RE, Wang ML. Targeting Bruton's tyrosine kinase with ibrutinib in B-cell malignancies. Clinical pharmacology and therapeutics. 2015;97(5):455-68.

116. Furman RR, Cheng S, Lu P, Setty M, Perez AR, Guo A, et al. Ibrutinib resistance in chronic lymphocytic leukemia. The New England journal of medicine. 2014;370(24):2352-4.

117. Tan SL, Liao C, Lucas MC, Stevenson C, DeMartino JA. Targeting the SYK-BTK axis for the treatment of immunological and hematological disorders: recent progress and therapeutic perspectives. Pharmacology & therapeutics. 2013;138(2):294-309.